Initial experimental evaluation of crud-resistant materials for light water reactors

Citation: Dumnernchanvanit, I., et al. "Initial Experimental Evaluation of Crud-Resistant Materials for Light Water Reactors." Journal of Nuclear Materials, 498 (January 2018): 1–8 © 2017 Elsevier B.V.

As Published: http://dx.doi.org/10.1016/j.jnucmat.2017.10.010

Publisher: Elsevier BV

Persistent URL: https://hdl.handle.net/1721.1/123982

Version: Original manuscript: author's manuscript prior to formal peer review

Manuscript Details

Manuscript number	JNM_2017_554
Title	Initial Experimental Evaluation of Crud-Resistant Materials for Light Water Reactors
Article type	Full Length Article

Abstract

The buildup of fouling deposits on nuclear fuel rods, known as crud, continues to challenge the worldwide fleet of light water reactors (LWRs). Crud causes serious operational problems for LWRs, including axial power shifts, accelerated fuel clad corrosion, increased primary circuit radiation dose rates, and in some instances has led directly to fuel failure. Numerous studies continue to attempt to model and predict the effects of crud, but each assumes that it will always be present. In this study, we report on the development of crud-resistant materials as fuel cladding coatings, to reduce or eliminate these problems altogether. Integrated loop testing experiments at flowing LWR conditions show significantly reduced crud adhesion and surface crud coverage, respectively, for TiC and ZrN coatings on stainless steel. The loop testing results roughly agree with the London dispersion component of van der Waals theoretical force predictions, suggesting that they contribute most significantly to the adhesion of crud to fuel cladding in out-of-pile conditions. These results motivate a new look at ways of reducing crud, thus avoiding many expensive LWR operational issues.

Manuscript category	Nuclear materials, fuels and waste materials
Corresponding Author	Michael Short
Order of Authors	Ittinop Dumnernchanvanit, Naiqiang Zhang, Sean Robertson, Alexandra Delmore, Max Carlson, Dennis Hussey, Michael Short
Suggested reviewers	Annalisa Manera, Barclay Jones, Hirotaka Kawamura, Gregory Lefevre, Jim Henshaw

Submission Files Included in this PDF

File Name [File Type]

IHTFP-Loop-Testing-Cover-Letter - Revision.pdf [Cover Letter]

JNM-Reviewer-Response.pdf [Response to Reviewers]

CRUD-Resistant-Materials_-
_Loop_Testing - Change Tracked Revision.pdf [Revised Manuscript with Changes Marked]

CRUD-Resistant-Materials_-_Loop_Testing - Clean Revision.pdf [Manuscript File]

Submission Files Not Included in this PDF

File Name [File Type]

TeX Source.zip [LaTeX Source File]

2017-IHTFP-Loop-Testing-dataprofile.xml [e-Component]

To view all the submission files, including those not included in the PDF, click on the manuscript title on your EVISE Homepage, then click 'Download zip file'.

Research Data Related to this Submission

There are no linked research data sets for this submission. The following reason is given:
Our data repository is hosted by Zotero, which is not on the drop-down list of data repositories available from the Elsevier submission system. See reference [42] in our manuscript for the link.

Michael Short
Assistant Professor
Department of Nuclear Science and Engineering
Massachusetts Institute of Technology

NSE
Nuclear Science and Engineering
science : systems : society

web.mit.edu/nse
77 Massachusetts Avenue
Room 24-204
Cambridge MA 02139
617.347.7763
hereiam@mit.edu

August 9, 2017

To the Editors of the Journal of Nuclear Materials,

Please find enclosed our revised manuscript, entitled “Initial Experimental Evaluation of Crud-Resistant Materials for Light Water Reactors.”
This represents the first experimental study to our knowledge of whether van der Waals (VDW) forces can be used to reduce or eliminate the formation of crud in pressurized water reactors (PWRs). Much work has been undertaken in the past thirty years, most notably in the Consortium for the Advanced Simulation of Light Water Reactors (CASL), to precisely predict the locations, magnitude, and effects of crud deposition. Strikingly few studies have focused on the total elimination of crud deposits. This study represents the first openly published experimental measurements of the relative crud resistance of different materials in flowing PWR conditions. The support of its hypothesis by the results within suggest that we can use the Hamaker constant of van der Waals forces (VDW) to design effective crud-resistant fuel coatings.

Summary of Revisions: We have done our best to respond to each of the two reviewer’s suggested concerns. In many cases this resulted in changes to the manuscript, which can be most easily seen in the change-tracked version. For others, rebuttals or explanations are given with references to outside studies, specific lines in the original manuscript, or other information about the experiments. We wish to point out that we are most interested in the *relative* fractions of crud coverage on each sample’s coated and uncoated regions, not absolute crud coverage fractions between experiments. We have done our best to explain why this is the case. In addition, we are requesting clarification of point #11 from Reviewer 2, concerning “removal of substrate material.” We have done our best to guess what this may refer to, but we recognize that we may have misinterpreted the statement. A clarification would be appreciated, so we can best respond to the suggestion of the reviewer.

Motivation: The formation of fouling deposits continues to affect many industries, costing the U.S. alone up to 0.25% of its GDP by recent estimates. In the nuclear industry the formation of crud, a form of fouling, presents a host of major operational issues, ranging from axial power offsets to increased primary side worker dose to causing fuel failure by a few different mechanisms. Crud is conservatively estimated to cost every PWR in the U.S. about $1.8 million per fuel cycle. $1M of this comes from ultrasonic fuel cleaning, which right now is only 40-60% efficient. This mostly comes from the cost of renting the machine and additional outage downtime. Another $800k is estimated in lost power from using a less aggressive fuel loading scheme, which is the primary way that crud is reduced in PWRs in the US. This does not take into account additional costs in worker dose, power downgrades due to axial offset (which have reached up to 25% in some US plants recently), or sudden outages due to fuel failures. Were the problem of crud to be eliminated, it would greatly improve the reliability and economics of PWR operation. This study also has the ability to impact many other industries which suffer similar fouling caused by the same underlying mechanisms.

Synopsis of Results: We have constructed a flowing PWR-like loop, the Internally Heated Testloop For PWRs (IHTFP), to simulate the conditions inside a PWR without the radiation. The same pressures, temperatures, water chemistries, fluid flow, and other parameters are achieved, with the caveat of a lower cladding heat flux due to the choice of an electrically isolated heating cartridge. This, in contrast to other loops like the Westinghouse WALT loop, deliberately avoids applying a voltage to the water-contacting clad face to avoid changing the surface electrochemical potential. It was hypothesized that London dispersion component of VDW forces, or the induced-dipole-induced-dipole forces between non-charged surfaces, dominate the energetics of the initial phase of crud deposition. Nine potential coatings were chosen for their varying visible refractive indices (an approximator for the Hamaker constant of proportionality for VDW forces), among other PWR-relevant material selection criteria. Two materials, ZrN and TiC, reduced crud accumulation as measured by surface coverage compared to a control area on each sample by 40% with 95% confidence. A strong correlation was found between the UV index of refraction and the crud reduction, as the Hamaker constant can be approximated by a single UV oscillation frequency version of the full spectral Hamaker constant formula.

Significance of Results: We conclude noting the strong correlation between the UV-approximated Hamaker constant and as-measured crud surface coverage reductions. This suggests that indeed London dispersion forces are most important in determining crud adhesion, and that calculations of VDW forces from Lifshitz theory (following the work of Lefèvre and Jolivet in 2009) should predict the crud resistance of new coatings. This assumes other relevant material selection criteria, such as low neutron cross section, ease of manufacture, and compatibility with PWR water undergoing radiolysis, are met. This result carries significant implications for other similar industries, such as downhole geothermal wells, heat exchangers, and boiler systems, all of which suffer from crud-like fouling deposits. The first to benefit may be boiling water reactors (BWRs), which suffer from significant crud problems of their own.

Future of This Work: A more detailed study using an atomic force microscope (AFM) is underway to experimentally verify calculated or approximated Hamaker constants, and to see the magnitude of DLVO forces relative to London dispersion forces in crud adhesion. A high-pressure, high-temperature AFM is under construction to perform these studies directly in PWR conditions. Finally, the three most promising coatings from all of our studies will soon be irradiated in the MIT reactor, to investigate surface chemical changes upon exposure to radiolysis in an in-pile PWR loop. Should all these tests prove successful, a number of lead test rods are planned for a 2019 campaign to see if they really work in a commercial PWR.

Thank you for your re-consideration of our manuscript for publication in the Journal of Nuclear Materials. If you have any questions regarding our submission, please contact us using any of the methods above.

Sincerely,

Michael Short

We thank the reviewers and the editor for their thorough feedback on our manuscript. We have done our best to address all the proposed changes and suggestions. Each one is detailed below, and we have included a change-tracked manuscript for verification of satisfactory changes. Indeed the suggestions have helped us to refine the accuracy of our claims, specify exactly how reactor-like our IHTFP loop really is, and mention the future work already underway to continue testing our potentially crud-resistant coatings.

Comments from the editors and reviewers:
-Reviewer 1

Two major comments:

1. Crud deposition is highly dependent on degree of local sub-cooled boiling or steaming. You point out that the test conditions are for significantly lower heat flux and flow than is typical in a PWR and say you are likely ignoring any soluble crud deposition mechanism (lines 264-265), implying no sub-cooled boiling, yet you suggest in a number of places that sub-cooled nucleate boiling is occurring (lines 385, 527). Please identify the degree of sub-cooled boiling or steaming that is occurring in your tests, e.g. using the Thom correlation, if applicable. If sub-cooled nucleate boiling is not occurring in your tests, please clearly state that, and remove your various references to sub-cooled boiling. Further, if sub-cooled nucleate boiling is only affecting certain samples or is varying in degree over certain samples, please clearly identify which samples are affected and to what degree.

The reviewer is right to request more specific information to prove (or disprove) whether sub-cooled boiling is indeed taking place. Using the Thom correlation[1], we find the following:

$$\Delta T_{sat} = 22.5 * \sqrt{q} * e^{(-P/8.7)}$$

Where ΔT_{sat} is in Kelvin, q is the heat flux in MW/m^2, and P is the system pressure in MPa. Using values of 0.206 MW/m^2 (65,302 BTU/hr ft^2) for the heat flux and a system pressure of 11.5 MPa in the tests in this paper (we had to lower it to avoid sudden heater rod burnout, and it also helped enhance boiling), we arrive at a ΔT_{sat} of 2.7 Kelvin (6.9 F). Given a liquid at saturation temperature ($T_{sub} = 0$), a wall superheat of only 1 Kelvin is required to induce sub-cooled boiling[2]. Our system was kept at/near saturation for the duration of the test, subcooled by just a few Kelvin to avoid circulation pump cavitation. This is still expected to be just above the threshold for sub-cooled boiling to occur. Finally, as direct evidence of sub-cooled boiling, experiments at the same conditions for longer times (part of a parallel effort) grew crud with many boiling chimneys. We have added these calculations and references to the manuscript. See below for a couple example images of the crud grown in the IHTFP loop, one of which we put in the manuscript as direct evidence of boiling chimneys in our crud:

[1] N. E. Todreas and M. Kazimi. "Fundamental of Heat and Mass Transfer: Volume I." CRC Press (2012).
[2] S. G. Kandlikar. "Heat Transfer Characteristics in Partial Boiling, Fully Developed Boiling, and Significant Void Flow Regions of Subcooled Flow Boiling." *J. Heat Transfer* 120(2), 395-401 (1998).

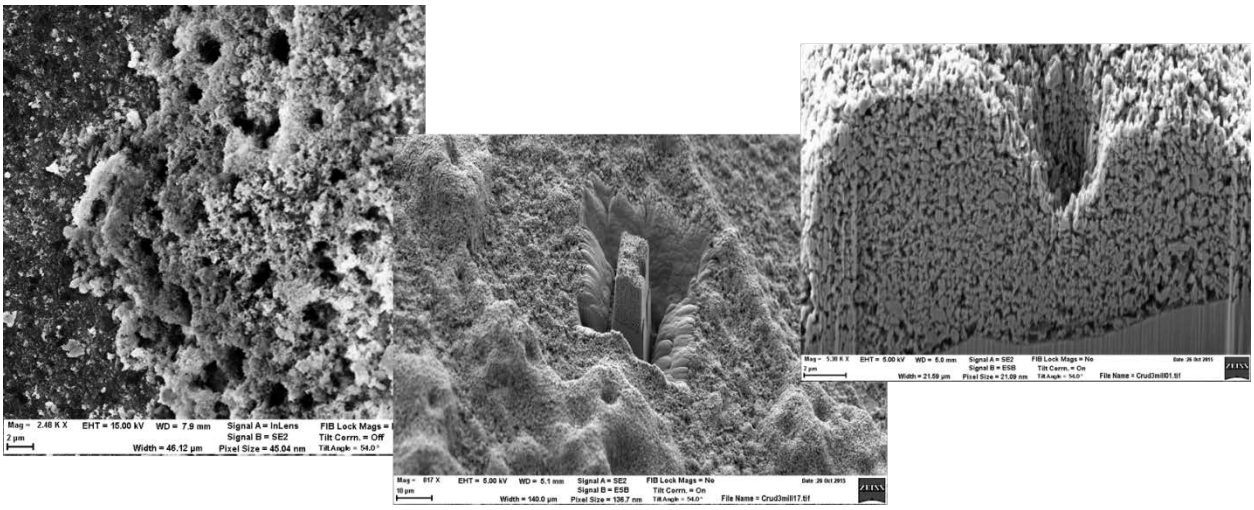

Figure 1: Examples of crud grown in the IHTFP loop, showing FIB cross sectioning of one of the boiling chimneys

In addition, we do not believe that there will be no sub-cooled boiling in the absence of soluble species, as the nanoparticulates which we added to our loop can also get trapped in the fluid microlayers underneath sub-cooled bubbles, which dry out to deposit the initial layers of crud. As for which samples experienced sub-cooled boiling, they likely all did, as relatively similar surface coverages (many tens of percent) were found on every control and coated surface of every sample.

2. Your conclusion includes suggestions for improvements to and further testing. However, you are silent on a recommendation for taking the next step to validate the crud resistant coatings that you identified in your tests. Please either recommend the next step with the specific crud resistant materials you identified or tell the reader why you do not think that next step should be taken yet.

Thank you for this suggestion, we have added a more substantial future work section explaining the ongoing and planned efforts to bring these crud resistant materials from the laboratory to commercial reactors.

Number of minor comments, in no particular order:

3. Abstract. Please remove the phrase "unpredictable and". The industry has spent a good deal of money and has been marginally successful in learning how to control crud in reactor.

Accepted this suggestion, thank you for noticing it.

4. Background lines 190-193 and Sample Preparation lines 223-224. You give limited explanation why you chose these nine materials for testing. To seriously pursue these coated materials for in reactor use, please more fully explain why these are good candidate materials.

Thank you for this suggestion. We chose most of the materials (Zr and Ti compounds) for their low thermal neutron cross sections, chemical compatability with the eventually underlying ZIRLO cladding, high hardness (to avoid fretting), and varying surface energies. This last

criterion is why we included Al_2O_3 and MgO, as they represent high and low surface energies. It was initially hypothesized that surface energy would be the controlling criterion for crud resistance, but that proved to be false. When searching for a better explanation, we came upon the Hamaker constant through the work of G. Lefevre and A. Jolivet (ref. [41]), among others, which guided our studies. We have added an explanation of why we chose the considered materials in the manuscript.

5. Sample preparation line 226. 316 stainless was used for the rings. Why?

The simple answer is that we ran out of ZIRLO (see the numerous burned out heating rods mentioned above), but the real technical answer is that we were only testing the crud-resistance (adhesion strength) to the coating itself. As mentioned in line 235 of the original submission, once the coating becomes ~10nm thick, the surface chemistry and adhesion become completely independent of the substrate at short particle-coating separation distances. This is because of the short-range nature of van der Waals (VDW) forces, whose effects are only felt strongly on the single nanometer scale, and drop off with distance squared for the case of a sphere (an approximation of a crud particle) in contact with a flat surface. For example, on page 255 of Israelachvili's book (ref. [22] in the original submission), the pressure exerted by a sphere on a flat surface drops in magnitude by 10^5 at a distance of 10nm. While it is true that VDW forces are dominated by the substrate in a coated system at large separation distances (pp. 282-283 of Israelachvili), the magnitudes of these forces are so small that turbulent forces far outweigh them until they come very close the surface, less than 10nm away. It has also been shown that VDW forces are dominated by the coating, not the substrate, for separation distances on the order of or smaller than the coating thickness. We have added this last note to the manuscript. This holds true even for adsorbed monolayers on other materials (a side note, see Israelachvili's book Ch. 13).

Therefore, we firmly believe that the underlying substrate does not matter in these measurements, provided adequate coating adhesion to the substrate continued to exist.

6. Sample Preparation lines 227-236. Why was a very smooth substrate surface used? This is not typical of cladding used in reactor. It would be preferable to use surface finishes typical of cladding used in reactor, as surface finish may influence crud deposition. However, if you need the smooth surface for the PVD, then at least state that. And, you make a statement regarding necessary coating thickness to avoid changing adhesion. Please identify more clearly what that issue is.

A smooth surface was not used for the PVD, but rather to separate any effects of variable surface roughness on the results. While the IHTFP loop tests are integrated by nature, we still sought to control as many variables as we could. Our lab-scale studies in the atomic force microscope (AFM) showed huge variability in adhesion values with rough substrates, while smooth substrates exhibited far better statistics. Therefore, we wanted to test only the effect of surface chemistry, and exclude roughness. Please see the above comment and the changes made around line 235 for a reply to the second half of this statement.

Please also note lines 227-229, where we mention the following: "The rings were mechanically and electrochemically polished to a mirror finish of <50 nm…" Therefore, we did indeed start with a mirror-smooth surface for the PVD, but it is not required. This way, however, we ensure that we are studying purely the effect of surface chemistry, and not roughness in addition. Once

applied to cladding rods in a PWR, there will inevitably be small regions in scratches that are not coated by PVD, and that is OK. We're not even sure that PVD will be the final manufacturing process to be used in a commercial PWR, which will depend on which coating(s) make the final cut.

7. Sample Preparation line 247. Please insert "Table" before "2".

Thank you for catching this, we have corrected this omission.

8. Sample Preparation lines 249-251. The explanation that tiny variations in ring diameter lead to differences in thermal contact is disturbing without a more thorough explanation.

We agree that while this is unfortunate, there simply isn't much we could do within the limits of machining tolerances available (which are objectively quite good). Even though our calipers measured the same ring diameters and heater rod diameters, we felt tactile differences in the force required to slide each ring onto the heater rod. Each ring was machined to be ever so slightly narrower than the heater rod, to ensure that some elastic stretching would be required to (1) maintain ring-rod contact and (2) ensure as good of thermal contact as possible. The insides of each ring were also polished to remove surface asperities and further improve this thermal contact. Nevertheless, we felt a duty to report the difference in sliding friction that we felt when loading each ring onto the heater rod. We have added an explanation of how we noticed these differences in the manuscript.

9. Sample Preparation. Is there any dependence in operating characteristics or results based on position of the specimen rings on the test rod? Uniformity of operating conditions along the test rod should be addressed somewhere.

Good point, we had performed cursory CFD studies to ensure roughly similar flow rates for each ring location, especially considering the effect of the viewing windows in our autoclave. It was confirmed that the windows have a negligible effect on fluid flow, so that the flow along all rings is quite uniform[3]. Certainly the liquid temperature will rise a bit along the rod, though this cannot be avoided in this geometry. This is precisely why we coated only half of each specimen (see Figure 3 of the original submission), to correct for any location-dependent changes in bulk coolant temperature, heat flux, etc. The presence of significant surface coverage on every sample provides evidence that the conditions were quite similar at each location, and coupled with the knowledge of sub-cooled boiling (see question (1) above) we know that the conditions were similar enough.

10. Flowing PWR Loop Tests line 263. Remove duplicate phrase "were used".

Thank you for catching this, we have removed this duplicate phrase.

11. Flowing PWR Loop Tests line 257-265. The test operates with a low Reynolds number and mass flux compared to a PWR. And, you comment that the crud precursors are elevated, likely ignoring any soluble crud deposition mechanism. See the major comment about steaming above. But, in addition, arguments persist that flow erosion is effective in crud removal. If your crud deposition is mostly particulate and you have low flows, then

[3] I. Dumnernchanvanit. PhD Thesis, available at http://dpsace.mit.edu/ (2017).

crud erosion under normal PWR conditions might invalidate your findings. If possible, a brief rebuttal for that argument should be included.

Thank you for the suggestion to include a brief rebuttal to the argument of changing mechanisms. We do not believe that the lower Reynolds number nor the elevated crud precursors invalidate our tests. Indeed flow erosion is very effective at crud removal, as evidenced by the "striping" of crud directly after the spacer grids and mixing vanes observed in PWRs[4]. Our specific aim in these experiments was to accelerate the formation of crud *without changing the initial deposition mechanism*, by both increasing crud precursors and lowering flow (the first point we could control, the second we could not due to loop geometry). In addition, the loop is constructed out of 316 stainless steel, which provides a "natural" soluble crud source term in the form of iron and nickel release much like the hot & cold legs of a PWR. The inner surfaces of all our loop tubes are covered with a black oxide layer, providing evidence that continued corrosion and soluble metal release is occurring, even at spots where the oxide was cleaned off.

12. SEM Image Analysis lines 323-325. Could you use other techniques besides "by eye" to show that these imaging techniques really are reflecting the presence and absence of crud?

Very good point, the phrase "by eye" does not fully capture how we determined where crud did and did not exist. Analysis of the first few training images required us to zoom in to regions difficult to determine, like those in the upper-right portion of the left half of Figure 4. Then, we used EDX elemental analysis to see whether the features/particles we saw were rich in Ni and/or Fe, two elements not used in any of our coatings. Regions which contained significant Fe/Ni were deemed to be crud, which could have only grown from either the particulate precursors or soluble metal released, while lighter regions which did not contain Fe- or Ni-rich particles were deemed not to be crud. We have revised our manuscript to explain how we determined these regions.

13. Results lines 381-386. You're attributing the difference in surface coverage between the two tests to the thermal fit and differences in subcooled boiling needs more explanation. If this is the reason, it suggests rather significant differences in the amount of subcooled boiling between the two tests, which can play a major role in how your results should be interpreted. And, there were no other differences in how the first and second experiments were conducted?

We attribute the differences in *absolute* surface coverage between the two experiments to differences in the thermal fit and other parameters out of our control. However, we focus our meaningful results on the *relative* amount of crud on the coated side of each sample, compared to the adjoining uncoated side only. This way, the differences in the time of each experiment, amount of precursors, and slight differences in thermal fit can be ignored in the relative-only comparison. No other differences between the two experiments other than those reported in the original manuscript existed. In particular, system temperatures, heat fluxes, pressures, and water chemistries were carefully kept the same. In addition, the same ordering of the materials on the heater rod was used between the two tests.

---

[4] D. Walter et al., "High-Fidelity Simulation of Crud Deposition on a PWR Fuel Pin With Grid Spacers: A Proof-of-Principle using the Fully-Coupled MAMBA/DECART/STAR-CCM+ Code." NURETH-15, Paper NURETH15-551 (2013). available at http://www.casl.gov/docs/CASL-U-2013-0097-000.pdf

14. Conclusions and Future Work lines 523-527. You end by pointing out a need for understanding an instability in your coatings under subcooled boiling. See major comment on subcooled boiling. If your experiment has an issue with sample stability, you should be pointing that out earlier in the article. And, please consider a final article line that is not calling into question the validity of your tests.

Sample stability was not noticeably compromised in these tests, instead this sentence refers to the need to *confirm* whether materials are stable at different coating thicknesses. It is not yet known what the optimal coating thickness will be, and many of these materials are quite hard. While that may be a positive point from fretting resistance, if the coating becomes too thick it may be more susceptible to fracture and spalling. This sentence highlights the need to conduct these thickness studies, as they were not a part of our experiments.

In addition, we have taken the reviewer's suggestion to conclude our article with a preview of the future work we are conducting, focusing on the more positive aspects of the coatings to be tested. Thank you for this suggestion.

-Reviewer 2

-

Although it is very important to find some ways of reducing crud deposition on the fuel rods in PWRs, the manuscript – as ambitiously titled – does not answer this challenge. Not surprisingly, because it is a very difficult and complex task in nuclear power industry, as recognized by numerous Electric Power Research Institute meetings, reports, grants, and many other publications. In particular, the loop tests described in the manuscript have been already sponsored by three EPRI contracts.

Therefore, in reviewer's opinion, the more appropriate title of this manuscript would be:

Crud-Resistant Materials for Light Water Reactors: Very First Experimental Results, or: …….: Current Status of the Project

We see the reviewer's point, and have adjusted the title of the manuscript accordingly to be more accurate and less ambitious. We now refer to it as an "initial experimental evaluation of crud-resistant materials for PWRs," which is an accurate description of what was done in this study.

In the presence of sub-cooled nucleate boiling the formation and build-up of deposits on fuel rods can happen through various mechanisms, as discussed in the review paper co-authored by M.P. Short and D. Hussey (reference [9] in the manuscript). In the present phase of this project only one mechanism is being considered, namely adhesion of the NiO particles to the substrate through van der Walls forces. The authors also hypothesize "that matching the optical properties of fuel cladding coating to the surrounding water would impart resistance to the crud formation", but there are not enough certain data presented by them in the paper to confirm this statement.

The reviewer is correct, which is why we were quite careful not to claim that the hypothesis is correct and confirmed, but rather to say that "This hypothesis appears to have been supported by integral loop tests, and a qualitative comparisons of known, experimental refractive index spectra with that of water. (lines 507-510)" Referring to Figures 6-7, for all materials which have known UV indices of refraction, a strong inverse trend is seen between UV index of refraction and crud coverage fraction. In addition, many of the phases found in crud (NiO, Fe_3O_4, ZrO_2, Cr_2O_3) all possess similarly high Hamaker constants, suggesting that if VDW forces are the dominant force in crud adhesion (supported by the trend in Figure 6), then they should behave similarly to NiO. Furthermore, the actual foulant (whichever constituent crud phase adheres) will not matter according to VDW theory (see Equation 1), as if either material *a* (the coating) or material *b* (the crud) matches the optical properties of water, a zero Hamaker constant will be found. This has been experimentally confirmed for many sets of materials (see Israelachvili's book (Ref. [22]), Chapter 13, specifically Table 13.3 on p. 266) for examples and a review of such studies. In particular, note that PTFE (n=1.34), which has the same refractive index as water to within 1% (n=1.33), has one of the lowest Hamaker constants in the table. The same goes for silica (n=1.45) immersed in dodecane (n=1.421).

Therefore, our data *support* our hypothesis, which itself stems from experimentally derived theory. They do not yet *conclusively confirm* the hypothesis, but rather motivate more single-effect and integrated reactor testing. Both are currently underway, and will be the subject of future papers. We have also expanded the future work section to include this information.

In addition, upon further consideration of the reviewer's comment on soluble deposition, we can't be absolutely sure that it did not occur. We do note that the water-facing parts of all 316SS components in the IHTFP loop are covered in a black oxide, suggesting continued, slow corrosion and soluble metal release. In addition, the evolution of the crud precursor particles from their starting 8-20nm size to sizes ranging up to a few hundred nanometers suggests some soluble metal present, likely at the very low, but finite, concentrations of 1-3ppb for Ni and Fe according to EPRI's MULTEQ database[5], version 8.0.

The instrumental and experimental part of this project as described in the manuscript can be the subject of numerous questions and comments, such as:

1. Why stainless steel rings have been used as substrates and not more relevant Zircaloy-4, or other fuel cladding alloys used in PWRs? Are there any plans to use zirconium alloys as substrates in farther tests?

Please see our answer to point (5) of Reviewer 1 for a more complete explanation. In short, VDW theory predicts that (1) forces drop off by a factor of 10^5 about 10nm away from the surface, and (2) that the VDW forces are determined almost exclusively by a coating in a coating-substrate system up to separation distances equal to the coating thickness. We have also added some verbiage to the manuscript explaining this point for clarity. For our upcoming PWR-

[5] MULTEQ Equilibrium of an Electrolytic Solution with Vapor-Liquid Partitioning and Precipitation: The Database Version 8.0. EPRI, Palo Alto, CA: 2015. 3002005400.

flowing-loop in-reactor tests, we will be using ZIRLO substrates to avoid changing the water chemistry and for more realism.

2. Has fixing the 0.3 mm-thick rings by pressing been sufficient to assure the uniform heat flux between heating rod and rings? The authors posed this question themselves in lines 361 – 363.

We actually do not believe that uniform heat flux can possibly be obtained, due to differences in machining tolerances for each ring. Please see our answer to point (8) of Reviewer 1, both reviewers picked up on this point. This is the reason we used the half-coated sample geometry, so we could compare *relative* differences in crud coverage instead of absolute numbers. The relative differences on two halves of one sample should only be a function of the material vs. the substrate, while the absolute differences are also due to localized changes in heat flux and fluid flow conditions, in addition to absolute temperature along the rod. Therefore, we were careful not to make any claims about absolute coverage, nor do we think they are important to consider in this study.

3. The tests have been performed using "nanoparticle NiO crud precursor" (line 259) at weight concentrations in water of 27.5 ppm and 50 ppm in two experiments described. What was the size distribution of the starting nanoparticulate material? What was the concentration of nickel dissolved at the conditions of the test?

We used purchased 8-20nm NiO nanoparticles at the start of the test. It is interesting to note that the crud contains far larger particles than 8-20nm, indicating that the particles have grown or agglomerated somehow. As for the Ni concentration, it can only be very low, up to 1-3ppb as predicted by EPRI's MULTEQ thermodynamic database, version 8.0. Saturation is expected to be reached very quickly, within hours of loading the loop, based on previous EPRI and MAI experiments. We have added this information to the manuscript for clarity.

4. The concentration of NiO in the loop was up to 1000 times larger than in PWRs, as depicted in Figure 2. Are the processes of deposition at such high concentrations in the loop tests relevant to reactor conditions at all?

Yes, we believe them to be so. The concentration is still very low in an absolute sense, so that the particle suspension is still very dilute. As the mechanism of initial crud deposition is believed to be concentration of trapped species in the evaporating fluid microlayer underneath a bubble[6], more particles simply means a faster initial deposition rate. This is also why we were careful not to infer differences in crud growth rate, as we are only interested in its initial stages of formation.

5. Iron, which is the essential component of fuel crud in a form of mixed Ni-Fe spinel ferrites, as well as of bonaccordite Ni_2FeBO_5 in case of boron oxide anomaly, has not been added. Why not? Can the results of tests without Fe be meaningful? The presence of these compounds in PWR crud confirms that chemical reactions in the deposits play a big role, and that deposition of particles such as NiO is not an only process in crud formation.

[6] J. X. Chen. On the interaction between fuel crud and water chemistry in nuclear power plants. Technical Report SKI Report 00:5, Studsvik Material AB, SE-611 82 Nykoping, Sweden, 2000. SKI Report 00:5. (Ref. [19] in the manuscript)

We specifically sought to minimize the number of competing variables, which is why we used only one common crud precursor of NiO. Indeed there can be chemical reactions in the crud to form phases like bonaccordite (Ni_2FeBO_5), but these only occur at rather high temperatures starting at around 400C[7]. These can only be expected to form either in very thick crud[8] or during accident scenarios, and documentation of their findings is quite rare, though still present. Please see our response to the initial concerns of Reviewer 2 for why VDW theory predicts relatively little difference between the oxides to be present in PWRs, as all similar oxides with similarly high indices of refraction are predicted to be quite "sticky" by experimentally-validated VDW theory.

6. Have any SEM images of as prepared coatings been taken? Were the coatings of various compounds flat enough and non-porous? Didn't they crack and spall during pressing the rings to the heater? Are other techniques of measuring the thickness of deposits being considered?

SEM images of as-prepared coatings were taken on flat, polished substrates using a JEOL 5910 SEM. No discernable features were noticed during the SEM analysis, they were remarkably smooth. In addition, no porosity was observed. The thicknesses were approximate, as each sputtering target was calibrated by sputtering thicker films onto glass slides and measuring film thicknesses with optical equipment by the coating provider. We also attempted such thickness measurements on our as-received coatings using a Filmetrics white light interferometer, though the very thin nature (~50nm) of the coatings produced no reflection fringes, only a single curve. One must know the full refractive spectrum of these materials to determine the film thickness, or vice versa. Very few of these materials have refractive index data measured along the required spectrum of wavelengths, while some have no data except for points reported at 632.8nm or one other wavelength. Thus, we were not able to conclusively fit the white light curves to accurately determine film thickness. Additional investigations were attempted in a Zeiss NVision 40 dual beam SEM/FIB, but the layer was too thin to accurately measure beyond the tolerance stated by our coating provider. Therefore, we kept a nominal thickness of 50nm as provided to us. One could use secondary ion mass spectroscopy (SIMS), though this was prohibitively expensive and time-consuming, as MIT surprisingly does not have a SIMS system available.

Finally, while we could not directly investigate the states of the coatings while on the heater rod (it cannot fit in our SEM/FIB chamber), we did carefully analyze the coatings during image analysis. There were very few regions which appeared light at first, but turned out to be regions where the film had cracked (see the light patch in Figure 4 of the original manuscript, upper right corner of image for a representative example). Most images, however, showed no signs of cracking or spalling.

7. As listed in Table 3, the coverages on control substrates show very large differences, up to a factor of 2 especially in Experiment 1. Why so? Is it not related to some turbulence profile along heating rod? Or, different adherence of rings to the rod and heat flux irregularities?

---

[7] J. A.. Sawicki. "Evidence of Ni_2FeBO_5 and m-ZrO_2 precipitates in fuel rod deposits in AOA-affected high boiling duty PWR core." J. Nucl. Mater., 374(1):248-269 (2008).

[8] J. A. Sawicki. "Nuclear Chemistry Model of Borated Fuel Crud." AECL Tech. Report, INIS-FR-1554.

We believe this is partially due to unavoidable differences in thermal fit for each ring, as we could feel tactile differences between each ring and each rod. We machined the rings to as fine of a tolerance as we could, and even so the heater rods themselves have a finite machining tolerance. We did check the flow profiles of water in the loop and on the heater rod using CFD, and found no regions of particularly high turbulence. We were particularly concerned about flow near the autoclave windows, but in the end found little to no effect on the flow profile.

One other possibility exists – the second experiment, though longer, exhibited less crud overall. This may be partly due to the additional oxidation of the inner surfaces of the IHTFP loop, resulting in a decreasing soluble metal release source term with each successive experiment.

We are not so concerned with the *absolute* levels of crud coverage between experiments, but rather the *relative* amounts of crud coverage between one sample's coated and uncoated sides.

8. The results shown in Figure 5 may be very much dependent on the position of rings on the rod. What was the sequence of the test rings on the heating rod? Are they arranged in Figure 5 as in Figure 2?

The rings were positioned at the same spaces on the rod between the two experiments. However, the ordering in Figure 5 does not represent that in the image in Figure 2. One may notice that there are more than nine samples on the heater rod in Figure 2, as we took the opportunity to add a few more materials (like the Ti_2AlC MAX phase ring, second from left in Figure 2) for a couple other projects. Because they were not prepared in the same manner as the nine materials in our study, we could not include them in this manuscript, as the coating thicknesses and surface roughness differed too much from our nine chosen materials.

9. An added SEM figures comparing as deposited substrates, with the targets and controls prior and after exposure would be instructive and likely more useful than SEMs presented in Figure 4.

The SEM figures showed no discernable difference between coated and control regions on the as-coated samples. This is likely due to the very thin coatings used, which appear to be conformally applied. We felt that there was not much to learn from the images, therefore we elected instead to include those in Figure 4 to show a typical "difficult" image along with the results of all image processing algorithms attempted. This allows the reader to judge for his/herself whether we chose image processing algorithms well. As mentioned in point (6), we were not able to obtain SEM images of the sample rings on the rod itself, only after testing and removal from the heater rod.

10. Have any elemental EDX maps of Ni, Fe, and target metals been not taken? Particles shown in Figure 4 were as large as 1 μm compared to 50-nm thick substrates. Is it due do NiO particles aggregation or the reactions with the substrate material?

EDX analysis was performed on the set of ten images used to select the image processing algorithms to use. The particulate matter was indeed very rich in Ni, and occasionally contained noticeable Fe levels above those visible from the 316SS substrate beneath. The Ni is certainly due to the NiO intentionally added to the system, while the excess Fe likely came from oxide particles and/or soluble metal release from the inner 316SS surfaces of the loop apparatus. It is not known whether the observed, up to one micron particulates are due to particulate agglomeration in the fluid, or once they deposited as crud, or both. Nevertheless, the presence of

high levels of Ni was used in conjunction with SEM images of agglomerated particulates on the material surfaces to indicate the presence of crud.

11. In 27.5 ppm NiO test the crud coverages were markedly up to ~2 times larger than in 50 ppm NiO test?! This is a serious anomaly opposite to expectations. In addition, why some substrate material have disappeared? This may suggest that the conditions in loop have not been yet fully controlled. Additional experiments are needed and worth doing!!!!!

We agree, additional experiments are quite necessary, as we mentioned in the future work section. We have also amended the conclusions to reflect this need for additional experiments. As mentioned before, we are not so concerned with absolute levels of crud deposition, which could easily be due to slight differences in the tolerances of each sample ring and heater rod. We have added additional language at the end of the results section clarifying this point, thank you for pointing it out.

We do not understand the disappearance of substrate material that the reviewer mentions. Could he/she please clarify it in a separate author/reviewer correspondence? If it refers to the results in Figure 5 of the original manuscript, it should be noted that a negative "percent crud reduction" simply means that more crud was found on the coating *compared to the uncoated side* of the specimen. It is not a measure of substrate weight gain or loss.

12. In view of all experimental uncertainties noted, the Experiment 1 should be repeated with the rings repositioned in different sequence on heating rod. Confirmation that TiC and ZrN coatings on stainless steel are crud resistant would be very valuable, but must be confirmed by reproducibility of the results.

We completely agree with the reviewer's assertion that reproducibility is required, which is precisely why a battery of additional confirmatory tests is being performed. In particular, the flowing in-reactor tests of each material in coupon form will begin in October, and will include coupons of the four best materials exposed to flowing PWR water in the MIT reactor loop with radiolysis as PWR flux levels. These results will not be available for quite some time, and will be the subject of a future study. In the end, we believe that this more integrated test (in-reactor flowing loop test) with no difference in heat flux between specimens (gamma heating will be identical for each specimen) will provide the most commercial reactor-like study possible. Rather than repeat the out-of-pile loop tests, a suite of AFM measurements and in-reactor tests will confirm single-effect and integrated behavior, respectively. We have amended the future work section to mention these tests.

13. In PWR reactor operation local pH at the reactor fuel can be higher than 7.2 used in the tests. It is due to production of lithium in $^{10}B(n,\alpha)^{7}Li$ neutron capture reaction, especially at high boron concentrations during and after startups and near fresh loaded fuel.

This is true, though for consistency we kept our water chemistry as constant as we could, rather than adding Li throughout to simulate this process. For detailed recordings of instrument readings used to confirm this water chemistry, please see our GitHub data repository for this project (ref. [42] in the original manuscript). We (the authors) do not yet know whether elevated Li levels or pH on its own will change the crud deposition mechanism or rate, though someone in

industry may know. (We are aware that there is much we don't know, and are not allowed to know, in terms of industry LWR operating experience as members of academia).

14. Water temperature of 320°C and pressure of 15.5 MPa during tests are already fairly close to supercritical water conditions. Accelerated chemical reactions may start to play a significant role in hydrothermal formation of deposits and reactions with the substrate material, in addition or in place of van der Walls mechanism. Have any structural analysis of the deposits been performed, or will be?

We are very glad that you asked! A full structural analysis of the deposits formed in these and other IHTFP experiments is the subject of another paper, which we are preparing for publication. This includes SEM/FIB cross section analysis of thicker crud formed during longer experiments, along with analysis of the porosity, pore size distribution, and fractal dimensions to compare directly to PWRs and Westinghouse WALT loop crud experiments. More detailed chemical studies, such as x-ray diffraction (XRD), will help validate recent assertions of boron incorporation into the crud, as predicted in the third reference that Reviewer 2 mentioned (Z. Rak et al.). There, we are specifically looking to see if boron incorporates into NiO, or $NiFe_2O_4$ as predicted.

We actually begun writing up all these results into one paper, and at the 20 page mark we decided to split them into two distinct, independent stories, each with one central message. We have also added mention of this next set of studies, along with the references by Sawicki and Rak, to the future work section to mention which specific experiments and calculations we will be looking to confirm.

The authors also thank the reviewers for the reference by Frattini et al, which is a rare find of a public domain paper stating the severity and root cause of AOA (we have been looking for something like this for quite some time!). It has been added to the introduction, as proof of the severity and root cause of AOA (or CIPS) due to crud.

Some of the questions listed above could be at least partly addressed with reference to articles not cited in the manuscript:

P.L. Frattini, J. Blok. S. Chauffriat, J. Sawicki, J. Riddle, Axial offset anomaly: Coupling PWR primary chemistry with core design, Nuclear Energy 40(2) (2001) 123-135.

J.A. Sawicki, Hydrothermal synthesis of Ni_2FeBO_5 in near-supercritical PWR coolant and possible effects of neutron-induced ^{10}B fission in fuel crud, J. Nucl. Mater. 415(2) (2011) 179-188.

Zs. Rak, C.J. O'Brien, D.W. Brenner. D.A. Andersson, C.R. Stanek, Understanding the atomic level chemistry and structure of oxide deposits on fuel rods in light water nuclear reactors using first principles method, JOM 68(11) (2016); and some other publications by this group.

Please check carefully the list of references: Correct in it symbols of elements, spelling of names, …

Thank you for this suggestion, we have found numerous instances of acronyms or element names not capitalized, two misspellings of author names, and one missing issue number.

In Line 247: …"listed in 2". add Table before 2.

Thank you for catching this, we have added the missing label.

Initial Experimental Evaluation of Crud-Resistant Materials for Light Water Reactors

I. Dumnernchanvanit[a], N. Q. Zhang[b], S. Robertson[a], A. Delmore[a], M. B. Carlson[a], D. Hussey[c], M. P. Short[a,*]

[a] *Dept. of Nuclear Science and Engineering, Massachusetts Institute of Technology (MIT), 77 Massachusetts Ave., Cambridge, MA 02139*
[b] *Key Laboratory of Condition Monitoring and Control for Power Plant Equipment of Ministry of Education, North China Electric Power University (NCEPU), Beijing 102206, China*
[c] *Electric Power Research Institute (EPRI), 3420 Hillview Ave, Palo Alto, CA 94304*

Abstract

The buildup of fouling deposits on nuclear fuel rods, known as crud, continues to challenge the worldwide fleet of light water reactors (LWRs). Crud causes serious operational problems for LWRs, including axial power shifts, accelerated fuel clad corrosion, increased primary circuit radiation dose rates, and in some instances has led directly to fuel failure. Numerous studies continue to attempt to model and predict the effects of crud, but each assumes that it will always be present. In this study, we report on the development of crud-resistant materials as fuel cladding coatings, to reduce or eliminate these problems altogether. Integrated loop testing experiments at flowing LWR conditions show significantly reduced crud adhesion and surface crud coverage, respectively, for TiC and ZrN coatings on stainless steel. The loop testing results roughly agree with the London dispersion component of van der Waals theoretical force predictions, suggesting that they contribute most significantly to the adhesion of crud to fuel cladding in out-of-pile conditions. These results motivate a new look at ways of reducing crud, thus avoiding many ~~unpredictable and~~ expensive LWR operational issues.

1. Introduction

Among the many issues challenging light water reactor (LWR) operation, the buildup of corrosion deposits known as crud[1] continues to pose numerous operational and safety challenges for LWR operation [1]. These deposits have their origins in the internal surfaces of the reactor, which may exceed 30,000 m^2 for a commercial pressurized water reactor (PWR) [2]. Although the materials which comprise the hot/cold legs (304 stainless steel) and steam generators (Alloy 600 or 690) have very slow corrosion rates at PWR conditions [3, 4], their high surface areas release a significant amount of soluble and particulate materials into the primary circuit. These corrosion products concentrate on fuel rods, especially on locations where sub-cooled nucleate boiling occurs, growing porous corrosion deposits. Figure 1 shows an overview of the reactor system under consideration [5], along with a multiscale picture of crud corrosion deposits.

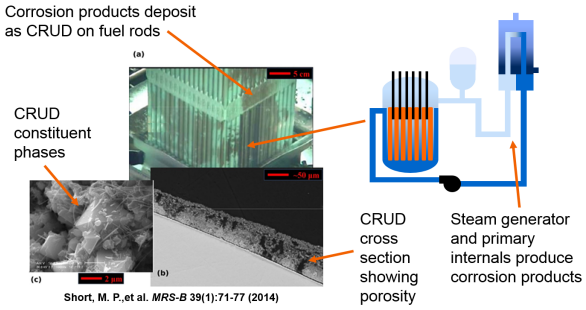

Figure 1: (Left) Multiscale view of crud [5], showing its highly porous structure. (Right) Diagram of a typical PWR primary loop, showing the source of crud (steam generator, hot/cold legs, core internals) and the location of deposition (fuel rods).

The porous nature of crud leads directly to many of the issues caused by its presence. In PWRs, the pores of the crud can concentrate soluble species normally present in the coolant, such as boric acid and lithium hydroxide [6], as well as trap radiolysis products formed by the splitting of water by ionizing radiation. This leads to aggressive chemical conditions such as elevated Li^+ concentrations and higher pH [7], which may contribute

*Corresponding author
Email addresses: ittinop@mit.edu (I. Dumnernchanvanit), zhnq@ncepu.edu.cn (N. Q. Zhang), srobertson@transatomicpower.com (S. Robertson), adelmore@mit.edu (A. Delmore), mc7@mit.edu (M. B. Carlson), dhussey@epri.com (D. Hussey), hereiam@mit.edu (M. P. Short)

[1] a bacronym for Chalk River Unidentified Deposits

to accelerated corrosion [8], ultimately resulting in fuel failure by crud-induced localized corrosion (CILC) in a number of notable cases [9]. Degraded heat transfer from fuel to coolant due to the presence of crud [10], which can reach a hundred microns in thickness, as well as elevation of the boiling point of water due to soluble species concentration [11] both increase cladding temperatures, thereby exponentially accelerating corrosion. Sudden dry-out from the increased pressure drop attributed to crud can also contribute to fuel failures. The same concentration of boron-bearing soluble species frequently causes a crud-induced power shift (CIPS) to occur, which has recently caused mandatory power deratings in plants ~~ranging from 3–15~~as high as 70% [1]. For a typical PWR operating at 1 GWe, this represents losses of $10,000 per day per percent power reduction. Shutdowns from a fuel failure may cost over $1,000,000 per day in lost electricity alone, in addition to required post-mortem fuel inspections and fuel reconstitution or replacement.

Of the current methods to prevent and deal with the formation of crud, increasing the number of feed assemblies to reduce the maximum steaming rate is the most frequently used in the industry. This is expensive and other technologies are considered to prevent this action. Ultrasonic fuel cleaning [12] has been used for over 15 years. This technology has the fuel assembly loaded into a chamber with banks of ultrasonic transducers that induce localized cavitation bubbles to dislodge the crud without excessively vibrating the fuel rods. The crud is removed by suction and collected in filters. Controlling water chemistry by zinc injection [13], electropolishing the fuel cladding to remove bubble nucleation sites [14], and pre-oxidation of the steam generator [15] to build up an oxide barrier have been considered and tested in the laboratory only. The ability to predict the locations and magnitude of crud buildup, while constantly improving using industry codes like EPRI's BOA [16] and CASL's MAMBA [17], is not high enough to adequately plan for its incidence. Therefore, solutions to completely eliminate the buildup of crud are sought to end these issues.

In this paper, we present experimental results to quantify the crud resistance of different potential fuel cladding coatings. These coatings, chosen for their surface chemical properties as well as their neutronic and chemical compatibility with conditions in a LWR core, were tested using an integrated flowing corrosion loop at PWR conditions to quantify relative amounts of crud surface coverage reduction. The results yield two candidate coatings, TiC and ZrN, which greatly reduce the buildup of crud. Van der Waals (VDW) theory is presented as an explanation for the results, and the data show enough agreement with theoretical predictions to suggest that VDW forces, specifically the induced-dipole force component, is the dominant mechanism of the adhesion of crud to fuel cladding and coatings.

2. Background

Crud, like all fouling deposits, must begin with the adhesion of a first layer to a clean substrate surface. In the case of nuclear reactor fuel, this substrate consists of zirconia (ZrO_2), in a mixture of its tetragonal and monoclinic forms. The crud itself consists mainly of nickel and iron oxides, in particular sub-stoichiometric trevorite ($NiFe_2O_4$), and nickel oxide (NiO) [18]. Reports of Ni metal [19], zirconia [20], and bonaccordite (Ni_2FeBO_5) [21] in PWR crud also exist. Specific material properties, such as the surface energy or the Hamaker constant [22], should dictate to what degree materials will adhere to each other in certain conditions should Debye forces or electrochemical double layers not significantly impact the result. Atomistic studies have provided insight as to whether these Debye forces or a combined DLVO force is required to describe the interactions between crud and fuel cladding. A study by Christensen and Carter [23] showed that the monoclinic ZrO_2 surface is unlikely to be solely cation or anion terminated, due to the long-range electrostatic forces that would render the surface metastable. It is these polar surfaces, charged predominantly with one sign or the other, that would induce the formation of an electrochemical double layer that could contribute noticeably to attraction or repulsion. One of the principal crud phases, NiO, has been shown to undergo octopolar reconstruction from a perfectly cation- or anion-terminated (111) facet, yielding nanofaceted regions 1.5 nm wide with opposite surface terminations [24]. These were deduced by studying the adsorption of NO to the NiO surface. Therefore, the area-averaged charge neutrality of both the monoclinic ZrO_2 and most stable NiO surfaces suggests that a net attraction or repulsion from an electrochemical double layer would not be a dominant force in crud adhesion.

The Hamaker constant A_{afb} describes the induced-dipole based adhesion by van der Waals (VDW) forces, in the case of two materials (a and b) interacting with an intervening fluid (f) [22]:

$$A_{afb} = \left(\sqrt{A_{ava}} - \sqrt{A_{fvf}}\right)\left(\sqrt{A_{bvb}} - \sqrt{A_{fvf}}\right) \quad (1)$$

where A_{ava}, A_{bvb}, and A_{fvf} are the vacuum Hamaker constants for material a, material b, and the fluid f respectively [25]. Calculations of these Hamaker constant is normally quite complex, requiring the application of full Lifshitz integrals [26]

and complete knowledge of the optical (dielectric, refractive) properties of each material [25]. However, simplifications can be made in certain circumstances, especially when the refractive index of all materials involved is relatively low, below 1.7 [27]. Using the Tabor-Winterton approximation (TWA) [28], each of these vacuum Hamaker constants can be written as follows [22], assuming the simplification of a single dominant electron oscillation frequency in the ultraviolet (UV) range [29]:

$$A_{ava}^{TWA} = \frac{3}{4} k_B T \left(\frac{\epsilon_a - 1}{\epsilon_a + 1} \right)^2 + \frac{3\pi\hbar\nu_e}{8\sqrt{2}} \frac{(n_a - 1)^2}{(n_a + 1)^{3/2}} \quad (2)$$

where k_B is Boltzmann's constant, T is the temperature in Kelvin, ϵ is a dielectric constant of a given material, $\hbar$ is Planck's constant, ν_e is the UV plasma oscillation frequency, and n is the index of refraction using the low-frequency limit of a material, taken in the visible-UV range [25]. Here the first term represents the zero-level energetic (electrostatic) contribution to adhesion, and is often ignored as its value rarely approaches over 5% of the Hamaker constant for a system without static charge, while the second term represents attraction or repulsion due to electron oscillations between the materials and the intermediating fluid or vacuum. The dielectric constant and refractive index of a vacuum, both unity, have been substituted here for simplicity. Finally, the Hamaker constant is directly proportional to the VDW force (F_{VDW}) between a spherical particle of crud of diameter d and a substrate, separated by a distance z, in any medium:

$$F_{VDW} = \frac{-A_{Ham} d}{6z^2} \quad (3)$$

Therefore, simply knowing the visible-UV refractive index of a material gives a hint as to whether it should be "sticky" or not. With a refractive index of 2.15 [22], ZrO_2 has a TWA vacuum Hamaker constant of 264.8 zJ, a considerably high value. This value corresponds well to the frequent observation of crud adhering to the zirconia scale always present on Zircaloy-based nuclear fuel rods. By contrast, the carbides and nitrides of Zr and Ti (which is chemically very similar to Zr) show considerably reduced refractive indices [30], and therefore likely lower Hamaker constants leading to less crud adhesion. Table 1 summarizes the known dielectric constants, indices of refraction, and vacuum Hamaker constants for a number of materials under consideration in this study, chosen for their high hardness, low neutron cross sections, and commercial availability. Long-term chemical compatibility with a PWR environment was considered, though not as strongly, so as to more expeditiously test the hypothesis of why crud sticks to fuel cladding. All of these coatings can be applied using conventional techniques, such as plasma ion infiltration or magnetron sputtering.

Material	$\mathbf{n_{633}}$	$\mathbf{n_{210}}$	$\mathbf{A_{ava}}$ **(zJ)**
H_2O, STP	1.332 [31]	1.41 [31]	37 [22]
H_2O, PWR	1.224 [32][1]	—	16.5
ZrO_2	2.24 [33][2]	2.39 [33]	270 [22]
ZrN	0.44 [34]	—	—
ZrC	—	—	—
TiO_2	2.583[35]	1.95 [36]	430 [22]
TiN [3]	1.351 [30]	1.89 [30]	—
TiC [3]	3.079 [30]	1.54 [30]	—
TiB_2	—	—	—
MgO	1.735 [37]	—	120 [38]
Al_2O_3	1.766 [39]	1.79 [39]	150 [22]

Table 1: Known optical properties for the materials in this study. n_{633} - Index of refraction at 633 nm. n_{210} - Index of refraction at 210 nm. A_{ava} - Vacuum Hamaker constant. [1]Quadratically extrapolated from liquid phase data at 320°C from [32]. [2]Data for monoclinic ZrO_2, average of two birefringent directions. "—" Not found or unavailable. [3]Data for the (111)-terminated face is used, according to [40].

It is unknown, however, whether a simple measurement of adhesion or Hamaker constant in standard laboratory conditions, whether in vacuum or in water, will translate directly to the desired engineering property of enhanced fouling resistance. One study by LeFevre and Jolivet has performed calculations to support this idea specifically in PWR conditions [41], but no study was found that experimentally tests it. They also explicitly note the surprising scarcity of full spectral refractive or dielectric data to perform these calculations. This study seeks to determine the fitness of predicting crud resistance by optical material properties, in an integrated test as similar to the environment found within a PWR as can be reasonably achieved.

3. Experimental Methods

All recordings from loop instrumentation, raw and processed data, spreadsheets for figure generation, and other files used in the creation of the results in this study can be found permanently hosted on our GitHub repository [42].

3.1. Sample Preparation

The nine materials given in Table 1 were chosen for all experiments in this study, based on chemical compatibility with Zircaloys, low neutron cross sections, high hardnesses, and representing a variety of surface energies. It was initially hypothesized that surface energy would be the controlling variable in determining crud resistance, this

Mat'l	$t_{sputter}$ (min.)	Ar (cm^3/min.)	O_2 (cm^3/min.)	N_2 (cm^3/min.)	RF (V)
ZrO_2	75	38	2	—	—
ZrN	15		—	2	-108
ZrC	7		—	—	—
TiO_2	108		2	—	—
TiN	18.75		—	2	-86
TiC	52.5		—	—	—
TiB_2	12.5		—	—	—
MgO	42		2	—	—
Al_2O_3	75		2	—	—

Table 2: PVD process parameters for each material used in this study

proved not to be the case. In all cases, test substrates were applied to 12.5 mm long, 17.5 mm inner diameter, and 0.2-0.3 mm thick 316 stainless steel rings for integrated flowing loop tests. The rings were mechanically and electrochemically polished to a mirror finish of <50 nm, and sonicated in acetone and ethanol for five minutes each to remove surface contaminants. Physical vapor deposition (PVD) was performed by PVD Products, Inc., to produce coatings roughly 50 nm thick. The exact coating thickness is unimportant provided that it is at least 10 nm thick, to avoid any effect of the underlying substrate changing adhesion. Israelachvili notes that VDW forces are dominated by the coating material in a coating-substrate system, for separation distances on the order of or smaller than the thickness of the coating [22]. Sputtering targets for each material were sourced with at least a 99.99% purity in the form of two-inch diameter discs 1/8th inch thick, bonded to a 1/8th inch disc of pure copper. All substrates were held at a distance of 3.5" from the sputtering target at room temperature, and utilized a 75 W radiofrequency (RF) source at 13.56MHz with a baseline pressure of less than $2.0 \cdot 10^{-6}$ Torr. Pressure was maintained at 5 mTorr for all depositions. Specifics for each material's PVD process parameters are listed in Table 2. Only one hemicylinder of each ring was coated, to ensure a built-in control surface on every specimen. This is due to tiny variations in ring diameter leading to differences in thermal contact, which despite our best efforts to make uniform within the tolerances of our machining tools, still resulted in slight differences in the tactile sliding friction when loading each ring onto the heater rod.

3.2. Flowing PWR Loop Tests

The newly constructed Internally Heated Testloop for PWRs (IHTFP) facility [43] was used for all flowing loop tests. Figure 2 shows a diagram and set of conditions used in the IHTFP, showing that all conditions except for Reynold's number and mass flux ~~were~~can be made identical to those found in PWRs. In these experiments, the system pressure was reduced to 11.5 MPa, resulting in a calculated water saturation temperature of 321C. This was done to avoid heater rod burnout, based on previous tests at 15.5 MPa experiencing such burnouts. Greatly increased nanoparticulate (8-20 nm) NiO crud precursor concentrations of 27.5 parts per million weight (ppmw) and 50.0 ppmw were used ~~were used~~ in the first and second experiments, respectively, to accelerate crud growth to the days-to-weeks timeframe~~, likely ignoring any soluble crud deposition mechanism~~. A pair of experiments were conducted at these conditions, one for four days, one for thirteen days.

The circulation water for these experiments was mixed in a 100 liter tank connected to the circulation loop. This was first filled with >15 MΩ/cm deionized water by evacuating the loop and using vacuum suction to draw the water in from the water storage tank, and then circulated through a mixed bed ion exchange filter and continuously measured until the water's electrical conductivity was below 0.09 μS/cm. The vacuum filling method was performed to ensure no gas bubbles would remain in the system, which would store energy when pressurized or interfere with measurement equipment. 99.999% dry argon was then bubbled through the tank until the dissolved oxygen concentration was maintained below 200 parts per billion (ppb). Then, 1,400 ppmw of boric acid was added to the tank, and LiOH was added until the pH of the solution reached 7.0. This amounted to 2.2 ppmw of LiOH during these tests. A Mettler-Toledo Thornton 770Max Pure Water Smart Sensor was used to measure pH, dissolved oxygen, and water conductivity. Water chemistry conditions were controlled and monitored according to the Electric Power Research Institute's (EPRI's) PWR water chemistry guidelines [44].

The IHTFP loop was heated using a combined 4,992 W of strip heaters and one vertical, internally heated, electrically isolated 1,750 W heater rod, yielding a nominal heat flux of 206 kW/m^2 during these tests. This is lower than the PWR core average, and is only suitable for relative comparisons of crud resistance, not absolute crud growth rates. Up to twelve different rings, each containing one half-coated ring of each material, were used to enable direct comparison of crud coverage for materials in identical test conditions. These half-coated samples were specifically used to correct for any slight differences in heat flux, thermal contact, flow velocity, or other localized environmental conditions. By comparing relative amounts of crud coverage between the coated and uncoated halves of each sample, the effectiveness of each coating at reducing crud surface coverage

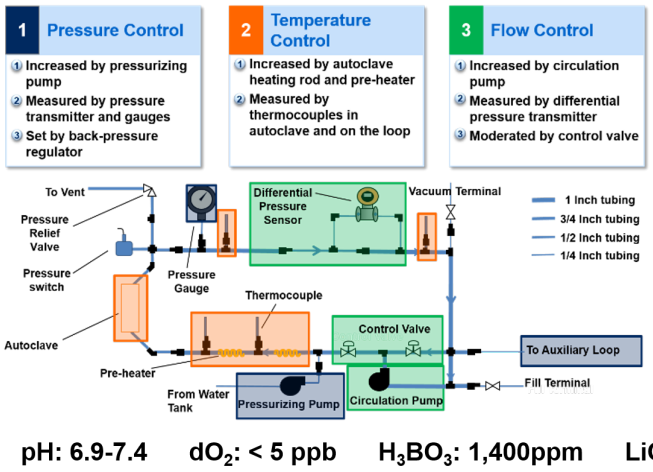

	PWR	IHTFP
Pressure	15.5 MPa	15.5 MPa
Temperature	287-324°C	320°C
Reynolds No.	$5 \cdot 10^5$	$1.62 \cdot 10^5$
Mass flux	3500 kg/m²s	1920 kg/m²s
Fe_3O_4, NiO	0.01 - 0.1 ppm	10 - 100 ppm

pH: 6.9-7.4 dO_2: < 5 ppb H_3BO_3: 1,400ppm LiOH: 2.2ppm H_2O Conductivity: <0.3 µS/cm

Figure 2: Diagram and experimental conditions in the IHTFP flowing tests

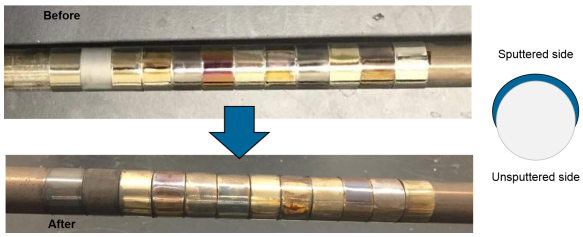

Figure 3: (Left) Images of specimen rings before and after the one-week tests, showing differences in crud coverage. (Right) Schematic showing how each specimen ring was half-coated, to ensure a built-in control surface for every specimen in every test.

can be more uniformly compared. Figure 3 shows images of the specimen rings on a heater rod, after press-fitting to ensure good thermal contact. Following flowing exposure in the IHTFP loop, specimens were extracted from the heater rod using a Dremel tool, and sectioned into control and coated halves near the control/coated delineation for scanning electron microscope (SEM) analysis.

The presence of sub-cooled boiling was confirmed using both calculations and direct experimental evidence. Kandlikar developed criteria for the onset of sub-cooled boiling [45], relating the system pressure, liquid sub-cooling, and flow parameters to the necessary wall superheat temperature. It can be seen that for reasonable surface roughness, only a 1°C wall superheat is required to induce sub-cooled boiling. In reality the IHTFP tests were conducted at 2-3°C to avoid circulation pump cavitation, still requiring a 1-2°C wall superheat. The superheat temperature of the samples in these experiments was calculated to be 2.7°C using the Thom correlation [46]:

$$\Delta T_{sat} = 22.5\sqrt{q''}e^{\left(\frac{-P}{8.7}\right)} \quad (4)$$

where ΔT_{sat} is the wall superheat in Kelvin, q" is

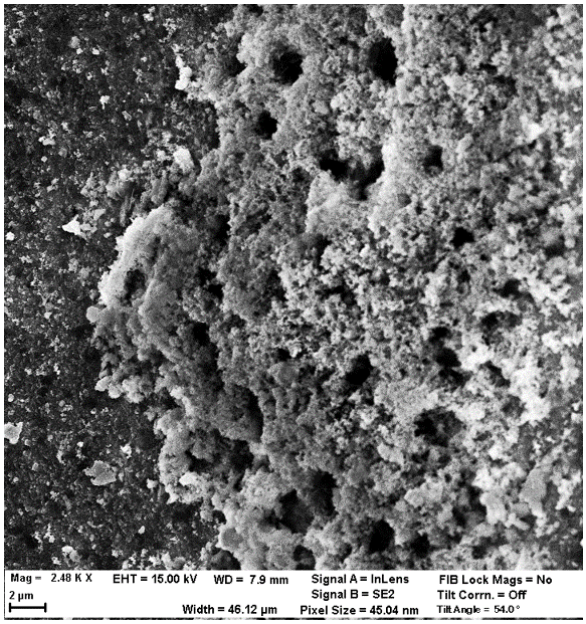

Figure 4: SEM image of crud grown in the IHTFP facility, exhibiting numerous boiling chimneys indicative of sub-cooled boiling

the heat flux in $^{MW}/_{m^2}$, and P is the system pressure in MPa. Therefore enough wall superheating exists to induce sub-cooled boiling. Direct experimental evidence of some of the thickest crud grown in these experiments (shown in Figure 4) also exhibits numerous boiling chimneys, which are direct evidence of sub-cooled boiling.

3.3. SEM Image Analysis

The goal of the image analysis was to quantify the relative percentage reduction in crud coverage between the coated and control surfaces of each specimen. To automate this process, image processing algorithms were used to binarize each

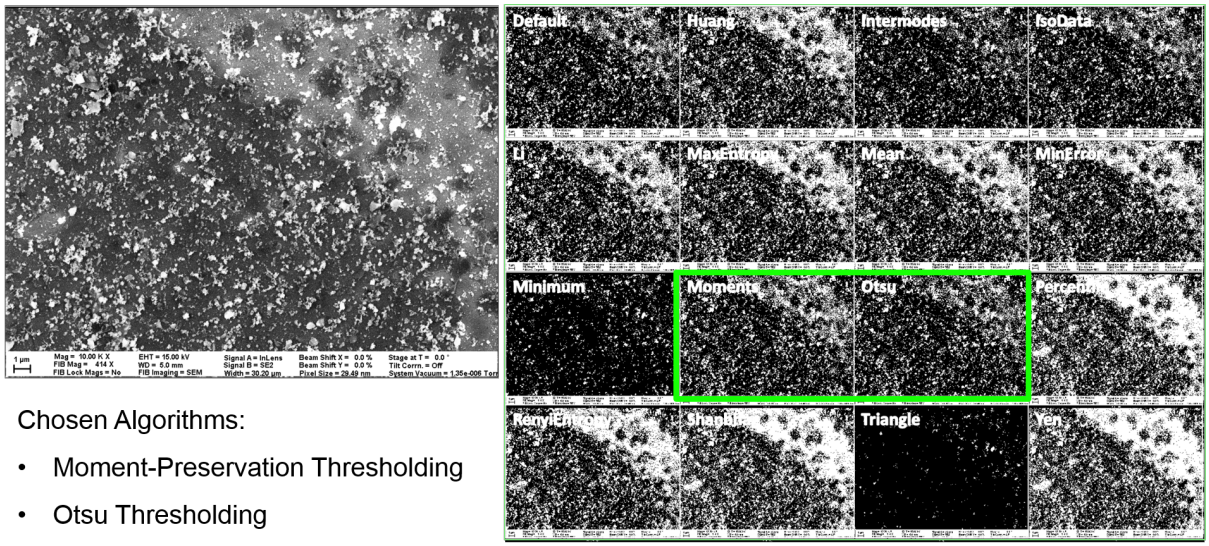

Figure 5: Example training image with binarized results from sixteen image processing algorithms

SEM image into crud and non-crud surfaces, allowing easy determination of how much crud existed on a surface. Sixteen image processing algorithms present in the ImageJ software package were tested using a series of five trial images from the complete dataset. The experimenters determined ~~by eye~~ which of the algorithms reliably binarized only the crud, and not other artifacts in the images, by training the sixteen image processing algorithms of a set of ten testing images. Zooming in to the light regions of each image revealed which areas contained crud-like small particulates, while EDX analysis in a JEOL 5910 SEM confirmed the presence of high levels of Ni, occasionally with Fe present. Regions without these two metals were deemed not to be crud, as none of the coatings contained them. Figure 5 shows this process in detail, revealing that the Moment Preserving [47] and Otsu [48] thresholding algorithms best isolated crud with minimal false positive identification of features. Ten SEM images at 10,000x magnification in secondary electron (SE) mode were taken using a Zeiss NVision 40 dual-beam SEM/FIB on each control and each coated surface of every specimen from both experiments, at distances at least one millimeter apart to ensure representative surface coverage. Both image processing algorithms were used to determine the percentage crud coverage on each material's coated and control surfaces. This was done to ensure that the choice of the image processing algorithm did not noticeably affect the results.

4. Results

Table 3 summarizes the crud coverage percentages for every control and coated surface in this study, while Figure 6 presents the results graphically. As can be seen in the figure, three materials reliably reduced the crud coverage fraction beyond experimental error. In the cases of TiC and ZrN, this reduction in coverage was 40%, a significant reduction in crud adhesion. Error bars in Figure 6 were generated by summing the averaged errors for each material's coated and control surfaces in quadrature, averaging across the two experiments, and doubling that value to obtain quadrature-averaged 95% confidence intervals. As should be expected, ZrO_2 showed no statistically significant change in crud coverage. Notable results include repeatable crud reduction with 95% confidence by ZrN, TiN, TiC, and repeatable increases in crud coverage by TiO_2, and MgO across both experiments and both image processing techniques. Two materials, ZrO_2 and Al_2O_3, showed an increase in crud coverage between coated and control surfaces in one experiment and a decrease in another. This may be attributable to different absolute heat fluxes between experiments, as each sample ring will have a sightly different dimension and therefore thermal fit. The doubled crud precursor concentration between experiments is not expected to noticeably affect results, and no significant deviation between experiments was observed. The choice of image processing never changed the sign of crud coverage except in the case of Al_2O_3, but not within the limits of experimental error. However, as can be seen in Table 3 and Figure 6 it did somewhat change the magnitude of observed crud coverage in some cases. This is why both were used, to ensure that the choice of image processing algorithm did not noticeably affect the final results. Finally, it should be noted that while the precursor concentration in the second experiment was almost doubled, abso-

	Experiment 1 (27.5 ppm NiO)				Experiment 2 (50.0 ppm NiO)			
Algorithm	**Moment Preserving**		**Otsu**		**Moment Preserving**		**Otsu**	
Material	Control	Coated	Control	Coated	Control	Coated	Control	Coated
ZrO_2	61.3 ± 7.9	51.4 ± 4.4	58.6 ± 7.9	46.8 ± 4.3	25.9 ± 2.5	36.2 ± 1.4	21.8 ± 4.3	27.3 ± 1.7
ZrN	47.0 ± 15.9	34.1 ± 3.9	45.8 ± 19.1	24.2 ± 4.8	31.2 ± 1.3	20.7 ± 0.2	22.2 ± 2.4	13.5 ± 0.6
ZrC	41.5 ± 11.8	33.2 ± 6.4	33.3 ± 10.1	32.4 ± 5.7	25.8 ± 0.4	23.9 ± 0.6	16.8 ± 1.0	15.7 ± 1.0
TiO_2	53.4 ± 3.6	54.0 ± 3.6	30.8 ± 4.5	52.9 ± 2.9	25.9 ± 0.4	33.7 ± 0.5	17.0 ± 1.3	22.1 ± 0.5
TiN	58.0 ± 9.3	49.1 ± 1.7	55.0 ± 10.4	47.6 ± 2.9	19.7 ± 0.2	16.6 ± 0.2	14.8 ± 0.9	12.4 ± 0.2
TiC	63.6 ± 11.0	44.6 ± 1.4	60.6 ± 13.3	43.2 ± 2.9	35.3 ± 6.3	18.4 ± 0.5	29.6 ± 8.2	13.8 ± 2.3
TiB_2	54.0 ± 2.9	62.9 ± 2.1	50.0 ± 1.9	58.7 ± 2.1	42.7 ± 8.1	44.9 ± 0.7	34.4 ± 8.3	37.2 ± 1.4
MgO	42.4 ± 2.4	49.7 ± 1.5	38.0 ± 6.4	47.0 ± 2.0	24.7 ± 0.5	33.5 ± 2.2	19.4 ± 0.9	24.8 ± 1.7
Al_2O_3	38.4 ± 5.7	45.1 ± 7.1	32.7 ± 5.4	43.0 ± 9.7	36.9 ± 8.3	26.2 ± 0.5	30.8 ± 8.6	21.8 ± 0.6

Table 3: Percentage crud coverages for all control and coated surfaces in this study, as measured by SEM and image analysis

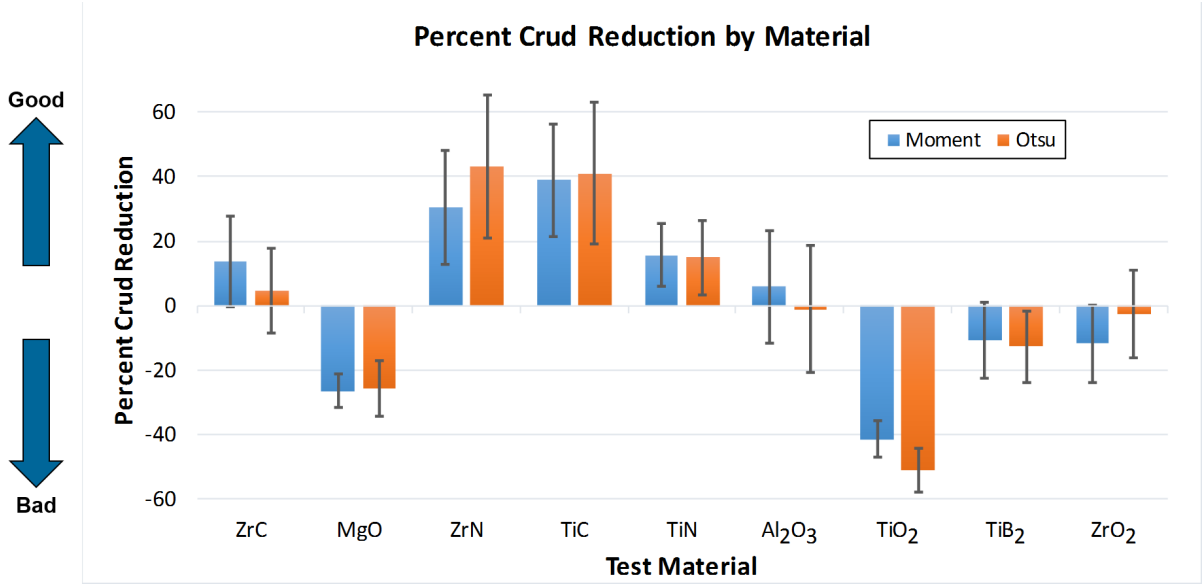

Figure 6: Relative reductions in crud coverage for the nine materials in this study, along with quadrature-averaged 95% confidence intervals in the measurements

lute surface coverages were uniformly lower. This can be attributed to either the continued passivization of the loop itself during operation, reducing the natural crud source term, or to differences in thermal fit and therefore sub-cooled boiling heat fluxes between experiments. It was noticed that each sample ring required a different sliding force to reach its position on the heater rod (all samples required considerable force to attach). Therefore, slight differences in the machined tolerances of each sample ring and each heating rod could have led to this difference in *absolute* crud coverage, by way of small differences in heat fluxes and wall superheat temperatures.

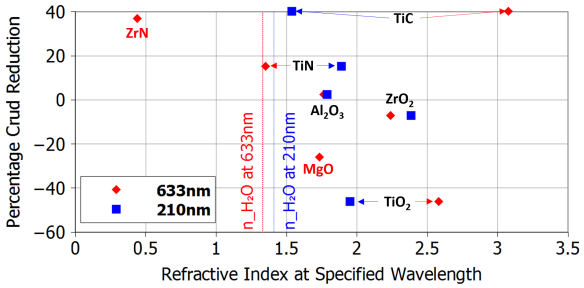

Figure 7: Comparison of percentage crud reduction in loop testing experiments vs. refractive index at two chosen wavelengths

5. Discussion

The data demonstrate that two materials, ZrN and TiC, were repeatably able to resist surface formation of crud in a PWR-representative environment by 40% with high confidence. One other material, TiN, performed satisfactorally within margins of error. The major conclusions are insensitive to the type of image processing algorithm used, and to the fluctuations in loop chemistry which are more extreme than those found in commercial PWRs. None of the other six materials tested resisted crud formation appreciably, while two (MgO and TiO_2) appeared to encourage it. TiO_2 has specifically been used to protect jet pump nozzle assemblies and inlet flow mixers in boiling water reactors (BWRs) [49], so its poor performance in this study raises the question of why it did not help. Dulka et al specifically used hard, electrically insulating ceramics such as TiO_2 and Ta_2O_5 to eliminate any electrostatic deposition of charged particulates floating in the BWR water, and it appears to have worked.

These data bring forth an obvious question: Do Van der Waals forces, specifically London dispersion forces, contribute most significantly to crud formation in PWRs? If the answer is yes, then it provides a convenient theoretical basis for the design of crud-resistant materials, provided the chosen materials are also hard, neutronically transparent, stable in PWR water, and resistant to radiation damage. The success of the work of Dulka et al does not preclude the existence of charged particulates in PWR water, which would interact with cladding materials via dipole-induced-dipole (Debye) forces, which are much stronger than induced-dipole-induced-dipole (London dispersion) forces. However, their study did demonstrate that these Debye forces can be masked using an electrical insulator, which is not highly electrostatically polarizable. In addition, the poor performance of TiO_2 in this study suggests a link between London dispersion forces and crud deposition, as masking the cladding in a manner nearly identical to that of Dulka et al did not prevent fouling.

A direct comparison of the percentage crud reduction with the visible refractive index, used in determining the TWA Hamaker constant, is given in Figure 7. A generally negative trend can be seen for the refractive index at both 633 nm (red) and 210 nm (ultraviolet) vs. the percentage crud reduction measured in this study, with one notable exception. Titanium carbide (TiC), despite having the highest refractive index at 633 nm, also demonstrated the most resistance to crud formation. All materials with tabulated data at a more ultraviolet wavelength of 210 nm (Al_2O_3, TiC, TiN, TiO_2, monoclinic ZrO_2) exhibited a marked negative correlation between refractive index at 210 nm and percentage crud reduction. This initially simple comparison points to more complexity required to fully explain the results.

The basis of the Tabor-Winterton approximation (TWA) is that for materials with low refractive indices (n<1.7), one can simply use a single value of the refractive index, commonly chosen at 633 nm (the emission line of a He-Ne laser), to approximate the full spectral Hamaker constant [27]. This has been verified by calculating both the TWA and full spectral Hamaker constants for a number of materials, and comparing with experimental measurements [22]. However, it appears that the TWA is really only valid for material-fluid-material systems whose indices of refraction vary in similar ways across the relevant parts of the spectrum, known to be the visible and ultraviolet ranges. A more detailed comparison of the refractive indices of seven of the tested materials whose refractive index spectra are known in this range is shown in Figure 8. Now the comparison becomes more clear, as the seven materials with known refractive index spectra roughly line up in order of increasing crud resistance vs. the difference in their UV refractive index spectra compared with water. In particular, TiC and ZrN show either near parity or a negative value in this relative refractive index spectrum in much of

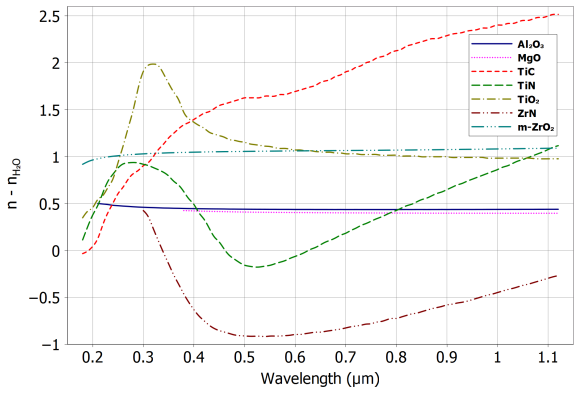

Figure 8: Comparison of percentage crud reduction in loop testing experiments vs. refractive index spectra in the visible and near UV/IR ranges. The difference in the refractive index vs. that of water for each material is plotted for a more meaningful comparison. Full spectral refractive index data sourced from [39] (Al_2O_3), [31] (H_2O), [37] (MgO), [30] (TiC & TiN), [36] (TiO_2), and [33] ($m - ZrO_2$), where 'm' stands for monoclinic.

the near-UV region, agreeing with previous studies suggesting that this near-UV region is quite important in determining the Hamaker constant [50, 25]. The negative relative refractive index of ZrN in particular suggests VDW repulsion at these wavelengths, which has been shown in previous systems [50]. This, combined with the previously stated evidence of static charges not being dominant when metallic surfaces are coated with electrical insulators [49], suggest that the induced-dipole component of VDW forces is the controlling variable in designing crud-resistant materials.

The major shortcoming in the current ability to design crud-resistant materials from theory is the availability of refractive index spectra in the near to far-UV range. Many of the data, despite being quite current, are simply not measured beyond the 100nm range due to the low wavelength cutoff of the deuterium arc lamp emission spectrum of 112 nm, the most common UV excitation source used in UV-vis-IR spectrometers. Either a lower wavelength UV source is required to determine these fuller refractive index spectra, or electronic excitation techniques such as valence electron energy loss spectroscopy (VEELS) can be used [51]. These measurements are quite feasible, it becomes a matter of turning our attention to experimental measurements of these and similar materials for the purpose of designing better crud-resistant material coatings.

6. Conclusions and Future Work

It was hypothesized that matching the optical properties of fuel cladding coatings to the surrounding water would impart resistance to crud formation. This hypothesis appears to have been supported by integral loop tests, and a qualitative comparisons of known, experimental refractive index spectra with that of water. In particular, TiC and ZrN were both found to reduce roughly 40% of crud deposition in two experiments with 95% confidence compared to uncoated control surfaces. Direct measurement of adhesion values in PWR-chemistry water and of the vacuum Hamaker constants of potential materials will confirm these integral tests and theoretical predictions, respectively. It is recommended to dedicate more resources to the experimental measurement of adhesion forces for these and similar coatings in the atomic force microscope (AFM), and to measure the refractive index spectra in the near-UV range (10-400 nm), to verify whether true full spectral refractive index comparison is a satisfactorally quantitative metric for designing crud-resistant materials. Future work should also consider determining the optimum thickness of the coatings/surface pretreatments to ensure the coating remains stable while the fuel rod heat flux sustains sub-cooled nucleate boiling.

The next steps for demonstrating the true effectiveness of these potentially crud-resistant coatings is in-reactor testing, where the material coatings, applied to prototypical ZIRLO or other Zircaloy coupons, will be exposed to flowing water at PWR conditions with radiolysis. This is a necessary step in testing crud resistance in a true reactor environment, as the coatings must both survive the test and continue functioning before testing as a lead test rod (LTR) could take place in a commercial reactor. These experiments are planned for the coming year, with an LTR campaign to follow in 2019 pending success. A parallel effort includes direct measurement of adhesion forces in the AFM, and the construction of a high-temperature, hyperbaric AFM for direct measurements of Hamaker constants in water at PWR conditions. Finally, continued analysis of the structure and chemistry of the crud formed in these experiments can help validate thermodynamic predictions, models of crud's effects, and experimental observations. These include the prediction that boron incorporates into the Ni-bearing phases of crud [52], verifiable by x-ray diffraction (XRD) analysis, cross-sectional fractal analysis of the structure of crud to validate assumptions made in models of crud's effects on cladding [53], and searching for phases like bonaccordite ($Ni2FeBO_5$) observed in PWRs [54].

Acknowledgments

Particular thanks are due to the Electric Power Research Institute (EPRI), for funding this work from its inception through loop testing under their

Polaris and PWR Technical Advisory Committee (P-TAC) programs on contract numbers 10002739, 10004433, and 10005086. Thanks are also due to the MIT Center for Advanced Nuclear Energy Systems (CANES), an MIT Energy Initiative (MITEI) Low-Carbon Energy Center (LCEC), for providing support for the loop testing autoclave, and to the MIT-Japan Hayashi Seed Grant for providing seed funds for this work. The authors also acknowledge James Greer and Adam Shepard from PVD Products, Inc. for sputtering services and disclosure of the PVD process parameters, and W. Art Byers, Zeses Karoutas, Guoqiang Wang, and Peng Xu of the Westinghouse Electric Company for many useful discussions.

[1] P. L. Frattini, J. Blok, S. Chauffriat, J. Sawicki, and J. Riddle. Axial offset anomaly: coupling PWR primary chemistry with core design. *Nucl. Ener.*, 40(2):123–135, 2001.

[2] A. Kunkle and D. Testa. The westinghouse pressurized water reactor nuclear power plant. Technical report, Westinghouse Electric Division, 1984. Accessed at http://www4.ncsu.edu/∼doster/NE405/Manuals/PWR_Manual.pdf on 2017-04-30.

[3] F. Carrette, M. C. Lafont, G. Chatainier, L. Guinard, and B. Pieraggi. Analysis and TEM examination of corrosion scales grown on alloy 690 exposed to pressurized water at 325°C. *Surf. Interface Anal.*, 34(1):135–138, 2002.

[4] R. Molins, M. Pijolat, M. Sennour, L. Marchetti, S. Perrin, and O. Raquet. Characterization of the oxide films formed at the surface of ni-base alloys in pressurized water reactors primary coolant by transmission electron microscopy. *Mater. Sci. Forum*, 595:539–547, 2008.

[5] M. P. Short, D. Gaston, C. R. Stanek, and S. Yip. A perspective on coupled multiscale simulation and validation in nuclear materials. *MRS Bulletin*, 39(1):71–77, 2014.

[6] J. Deshon, D. Hussey, B. Kendrick, J. McGurk, J. Secker, and M. P. Short. Pressurized water reactor fuel crud and corrosion modeling. *JOM*, 63(8):64, 2011.

[7] J. Henshaw, J. C. McGurk, H. E. Sims, A. Tuson, S. Dickinson, and J. Deshon. A model of chemistry and thermal hydraulics in PWR fuel crud deposits. *J. Nucl. Mater.*, 353(1-2):1–11, 2006.

[8] Y. H. Jeong, J. H. Baek, S. J. Kim, H. G. Kim, and H. Ruhmann. Corrosion characteristics and oxide microstructures of Zircaloy-4 in aqueous alkali hydroxide solutions. *J. Nucl. Mater.*, 270(3):322–333, 1999.

[9] J. Deshon et al. Fuel reliability guidelines: PWR fuel cladding crud and corrosion. Technical Report 1015499, Electric Power Research Institute (EPRI), Palo Alto, CA, USA, 2008.

[10] M. P. Short, D. Hussey, B. K. Kendrick, T. M. Besmann, C. R. Stanek, and S. Yip. Multiphysics modeling of porous CRUD deposits in nuclear reactors. *J. Nucl. Mater.*, 443(1-3):579–587, 2013.

[11] I. ul Haq, N. Cinosi, M. Bluck, G. Hewitt, and S. Walker. Modelling heat transfer and dissolved species concentrations within PWR crud. *Nucl. Eng. Des.*, 241(1):155–162, 2011.

[12] J. Blok, P. Frattini, D. Gross, and T. Moser. Advances in ultrasonic fuel cleaning. In *Proceeding of Societe Francaise d'Energie Nucleaire - SFEN, Fontevraud 5 International symposium*, 1-2, pages 547–553, Fontevraud - Royal Abbey (France), 2002.

[13] R. Yang, B. Cheng, J. Deshon, K. Edsinger, and O. Ozer. Fuel R & D to improve fuel reliability. *J. Nucl. Sci. Technol.*, 43(9):951–959, 2006.

[14] W. A. Byers, D. V. Paramonov, M. B. Dzodzo, Z. E. Karoutas, and M. Y. Young. Crud-resistant nuclear fuel cladding, 2004. U.S. Patent No, 6813329 B1.

[15] I. Bobin-Vastra, B. Sala, N. Engler, P. Saurin, and M. C. Thiry. Preoxidation of SG alloy 690 tubes to decrease metal release in the primary circuit: A laboratory study. In *8th International Symposium on Environmental Degradation of Materials in Nuclear Power Systems - Water Reactors*, volume 1-2, pages 507–513, Amelia Island, FL, USA, 1997. American Nuclear Society.

[16] EPRI. Boron-induced offset anomaly (BOA) risk assessment tool, version 1.0. Technical Report 1003211, Electric Power Research Institute (EPRI), Palo Alto, CA, USA, 2003.

[17] V. Petrov, B. K. Kendrick, D. Walter, A. Manera, and J. Secker. Prediction of CRUD deposition on PWR fuel using a state-of-the-art CFD-based multiphysics computational tool. *Nucl. Eng. Des.*, 299:95–104, 2016.

[18] J.-W. Yeon, I.-K. Choi, K.-K. Park, H.-M. Kwon, and K. Song. Chemical analysis of fuel crud obtained from korean nuclear power plants. *J. Nucl. Mater.*, 404(2):160–164, 2010.

[19] J. X. Chen. On the interaction between fuel crud and water chemistry in nuclear power plants. Technical Report SKI Report 00:5, Studsvik Material AB, SE-611 82 Nykoping, Sweden, 2000. SKI Report 00:5.

[20] J. A. Sawicki. Evidence of Ni2FeBO5 and m-ZrO2 precipitates in fuel rod deposits in AOA-affected high boiling duty PWR core. *J. Nucl. Mater.*, 374(1-2):248–269, 2008.

[21] J. A. Sawicki. Analyses of crud deposits on fuel rods in PWRs using Mossbauer spectroscopy. *J. Nucl. Mater.*, 402(2-3):124–129, 2010.

[22] J. N. Israelachvili. *Intermolecular and Surface Forces.* Academic Press, San Diego, third edition, 2011. pp. 261, 263, 275, 282-283.

[23] A. Christensen and E. A. Carter. First-principles study of the surfaces of zirconia. *Phys. Rev. B*, 58(12):8050, 1998.

[24] M. Schönnenbeck, D. Cappus, J. Klinkmann, H.-J. Freund, L. G. M. Petterson, and P. S. Bagus. Adsorption of CO and NO on NiO and CoO: a comparison. *Surf. Sci.*, 347(3):337–345, 1996.

[25] L. Bergström. Hamaker constants of inorganic materials. *Adv. Colloid Interface Sci.*, 70:125–169, 1997.

[26] E. M. Lifshitz. The theory of molecular attractive forces between solids. *Sov. Phys.*, 2(1):73–83, 1956.

[27] R. H. French, R. M. Cannon, L. K. DeNoyer, and Y.-M. Chiang. Full spectral calculation of non-retarded hamaker constants for ceramic systems from interband transition strengths. *Solid State Ionics*, 75:13–33, 1995.

[28] D. Tabor and R. H. S. Winterton. The direct measurement of normal and retarded van der waals forces. *Proc. R. Soc. London A: Mathematical, Physical and Engineering Sciences*, 312(1511):435–450, 1969.

[29] V. A. Parsegian. *Van der Waals Forces: A Handbook for Biologists, Chemists, Engineers, and Physicists.* Cambridge University Press, 2005. p. 63. ISBN 978-0511614606.

[30] J. Pflüger, J. Fink, W. Weber, K. P. Bohnen, and G. Crecelius. Dielectric properties of tic_x, tin_x, vc_x, and vn_x from 1.5 to 40 ev determined by electron-energy-loss spectroscopy. *Phys. Rev. B*, 30:1155–1163, 1984.

[31] M. Daimon and A. Masumura. Measurement of the refractive index of distilled water from the near-infrared region to the ultraviolet region. *Appl. Opt.*, 46(18):3811–3820, 2007.

[32] A. H. Harvey, J. S. Gallagher, and J. M. H. Levelt Sengers. Revised formulation for the refractive index of water and steam as a function of wavelength, temperature and density. *J. Phys. Chem. Ref. Data*, 27(4):761–774, 1998.

[33] N. M. Balzaretti and J. A. H. da Jornada. Pressure dependence of the refractive index of monoclinic and yttria-stabilized cubic zirconia. *Phys. Rev. B*, 52:9266–9269, 1995.

[34] M. Veszelei, K. Andersson, C.-G. Ribbing, K. Järrendahl, and H. Arwin. Optical constants and drude analysis of sputtered zirconium nitride films. *Appl. Opt.*, 33(10):1993–2001, 1994.

[35] J. R. DeVore. Refractive indices of rutile and sphalerite. *J. Opt. Soc. Am.*, 41(6):416–419, 1951.

[36] T. Siefke, S. Kroker, K. Pfeiffer, O. Puffky, K. Dietrich, D. Franta, I. Ohlídal, A. Szeghalmi, E.-B. Kley, and A. Tünnermann. Materials pushing the application limits of wire grid polarizers further into the deep ultraviolet spectral range. *Adv. Opt. Mater.*, 4:1780–1786, 2016.

[37] R. E. Stephens and Irving H. M. Index of refraction of magnesium oxide. *J. Res. Nat. Bureau Standards*, 49(4):249–252, 1952.

[38] L. Bergström, A. Meurk, H. Arwin, and D. J. Rowcliffe. Estimation of hamaker constants of ceramic materials from optical data using lifshitz theory. *J. Am. Ceram. Soc.*, 79(2):339–348, 1996.

[39] I. H. Malitson and M. J. Dodge. Refractive index and birefringence of synthetic sapphire. *J. Opt. Soc. Am.*, 62:1405, 1972.

[40] J. Rohrer and P. Hyldgaard. Ab initio thermodynamics of deposition growth: Surface terminations of TiC(111) and TiN(111) grown by chemical vapor deposition. *Phys. Rev. B*, 82:045415, 2010.

[41] G. Lefèvre and A. Jolivet. Calculation of hamaker constants applied to the deposition of metallic oxide particles at high temperature. In H. Müller-Steinhagen, M. R. Malayeri, and A. P. Watkinson, editors, *Proceedings of International Conference on Heat Exchanger Fouling and Cleaning VIII*, pages 120–124, Schladming, Austria, June 2009.

[42] [Dataset] I. Dumnernchanvanit, N. Q. Zhang, S. Robertson, A. Delmore, M. B. Carlson, D. Hussey, and M. P. Short. Data and code/script repository for 2017 IHTFP loop testing of crud-resistant materials paper, April 2017. GitHub repository. Accessible at https://github.com/shortlab/2017-IHTFP-Loop-Testing Permanent Link at DOI: 10.5281/zenodo.570008.

[43] I. Dumnernchanvanit, N. Zhang, A. R. Delmore, and M. P. Short. Design and assembly of experimental facility for CRUD characterization and mitigation at PWR cladding conditions. *Trans. Amer. Nucl. Soc.*, 111:1579–1582, 2014.

[44] J. Deshon et al. Pressurized water reactor primary water chemistry guidelines: Revision 7, volumes 1 and 2. Technical Report 3002000505, Electric Power Research Institute (EPRI), Palo Alto, CA, USA, 2014.

[45] S. G. Kandlikar. Heat transfer characteristics in partial boiling, fully developed boiling, and significant void flow regions of subcooled flow boiling. *J. Heat Transf.*, 120(2):395–401, 1998.

[46] N. E. Todreas and M. S. Kazimi. *Nuclear Systems Volume I: Thermal Hydraulic Fundamentals, Second Edition*. CRC Press, 2011.

[47] W.-H. Tsai. Moment-preserving thresholding: a new approach. *Computer Vision Graphics and Image Processing*, 19:377–393, 1984.

[48] N. Otsu. A threshold selection method from gray-level histograms. *IEEE Trans. Sys., Man., Cyber.*, 9(1):62–66, 1979.

[49] C. P. Dulka, J. F. Ackerman, D. W. Sandusky, M. O. Lenz, L. L. Lantz, M. B. McMahan, and G. A. MacMillan. Apparatus and methods for protecting a jet pump nozzle assembly and inlet-mixer, 2003. US Patent 6,633,623.

[50] J. Visser. On hamaker constants: A comparison between hamaker constants and lifshitz-van der waals constants. *Adv. Colloid Interface Sci.*, 3(4):331–363, 1972.

[51] R. H. French, C. Scheu, G. Duscher, H. Müllejans, M. J. Hoffmann, and R. M. Cannon. Interfacial electronic structure and full spectral hamaker constants of Si3N4 intergranular films from VUV and sr-veel spectroscopy. *MRS Proc.*, 357:243, 1994.

[52] Z. Rak, C. J. O'Brien, D. W. Brenner, D. A. Andersson, and C. R. Stanek. Understanding the atomic-level chemistry and structure of oxide deposits on fuel rods in light water nuclear reactors using first principles methods. *JOM*, 68(11):2912–2921, 2016.

[53] M. M. Jin and M. P. Short. Multiphysics modeling of two-phase film boiling within porous corrosion deposits. *J. Comput. Phys.*, 316:504–518, 2016.

[54] J. A. Sawicki. Hydrothermal synthesis of Ni2FeBO5 in near-supercritical PWR coolant and possible effects of neutron-induced 10B fission in fuel crud. *J. Nucl. Mater.*, 415(2):179–188, 2011.

Initial Experimental Evaluation of Crud-Resistant Materials for Light Water Reactors

I. Dumnernchanvanit[a], N. Q. Zhang[b], S. Robertson[a], A. Delmore[a], M. B. Carlson[a], D. Hussey[c], M. P. Short[a,*]

[a] *Dept. of Nuclear Science and Engineering, Massachusetts Institute of Technology (MIT), 77 Massachusetts Ave., Cambridge, MA 02139*
[b] *Key Laboratory of Condition Monitoring and Control for Power Plant Equipment of Ministry of Education, North China Electric Power University (NCEPU), Beijing 102206, China*
[c] *Electric Power Research Institute (EPRI), 3420 Hillview Ave, Palo Alto, CA 94304*

Abstract

The buildup of fouling deposits on nuclear fuel rods, known as crud, continues to challenge the worldwide fleet of light water reactors (LWRs). Crud causes serious operational problems for LWRs, including axial power shifts, accelerated fuel clad corrosion, increased primary circuit radiation dose rates, and in some instances has led directly to fuel failure. Numerous studies continue to attempt to model and predict the effects of crud, but each assumes that it will always be present. In this study, we report on the development of crud-resistant materials as fuel cladding coatings, to reduce or eliminate these problems altogether. Integrated loop testing experiments at flowing LWR conditions show significantly reduced crud adhesion and surface crud coverage, respectively, for TiC and ZrN coatings on stainless steel. The loop testing results roughly agree with the London dispersion component of van der Waals theoretical force predictions, suggesting that they contribute most significantly to the adhesion of crud to fuel cladding in out-of-pile conditions. These results motivate a new look at ways of reducing crud, thus avoiding many expensive LWR operational issues.

1. Introduction

Among the many issues challenging light water reactor (LWR) operation, the buildup of corrosion deposits known as crud[1] continues to pose numerous operational and safety challenges for LWR operation [1]. These deposits have their origins in the internal surfaces of the reactor, which may exceed 30,000 m^2 for a commercial pressurized water reactor (PWR) [2]. Although the materials which comprise the hot/cold legs (304 stainless steel) and steam generators (Alloy 600 or 690) have very slow corrosion rates at PWR conditions [3, 4], their high surface areas release a significant amount of soluble and particulate materials into the primary circuit. These corrosion products concentrate on fuel rods, especially on locations where sub-cooled nucleate boiling occurs, growing porous corrosion deposits. Figure 1 shows an overview of the reactor system under consideration [5], along with a multiscale picture of crud corrosion deposits.

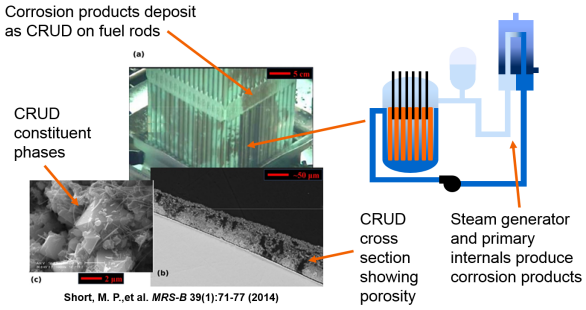

Figure 1: (Left) Multiscale view of crud [5], showing its highly porous structure. (Right) Diagram of a typical PWR primary loop, showing the source of crud (steam generator, hot/cold legs, core internals) and the location of deposition (fuel rods).

The porous nature of crud leads directly to many of the issues caused by its presence. In PWRs, the pores of the crud can concentrate soluble species normally present in the coolant, such as boric acid and lithium hydroxide [6], as well as trap radiolysis products formed by the splitting of water by ionizing radiation. This leads to aggressive chemical conditions such as elevated Li^+ concentrations and higher pH [7], which may

*Corresponding author
Email addresses: ittinop@mit.edu (I. Dumnernchanvanit), zhnq@ncepu.edu.cn (N. Q. Zhang), srobertson@transatomicpower.com (S. Robertson), adelmore@mit.edu (A. Delmore), mc7@mit.edu (M. B. Carlson), dhussey@epri.com (D. Hussey), hereiam@mit.edu (M. P. Short)

[1] a bacronym for Chalk River Unidentified Deposits

contribute to accelerated corrosion [8], ultimately resulting in fuel failure by crud-induced localized corrosion (CILC) in a number of notable cases [9]. Degraded heat transfer from fuel to coolant due to the presence of crud [10], which can reach a hundred microns in thickness, as well as elevation of the boiling point of water due to soluble species concentration [11] both increase cladding temperatures, thereby exponentially accelerating corrosion. Sudden dry-out from the increased pressure drop attributed to crud can also contribute to fuel failures. The same concentration of boron-bearing soluble species frequently causes a crud-induced power shift (CIPS) to occur, which has recently caused mandatory power deratings in plants as high as 70% [1]. For a typical PWR operating at 1 GWe, this represents losses of $10,000 per day per percent power reduction. Shutdowns from a fuel failure may cost over $1,000,000 per day in lost electricity alone, in addition to required post-mortem fuel inspections and fuel reconstitution or replacement.

Of the current methods to prevent and deal with the formation of crud, increasing the number of feed assemblies to reduce the maximum steaming rate is the most frequently used in the industry. This is expensive and other technologies are considered to prevent this action. Ultrasonic fuel cleaning [12] has been used for over 15 years. This technology has the fuel assembly loaded into a chamber with banks of ultrasonic transducers that induce localized cavitation bubbles to dislodge the crud without excessively vibrating the fuel rods. The crud is removed by suction and collected in filters. Controlling water chemistry by zinc injection [13], electropolishing the fuel cladding to remove bubble nucleation sites [14], and pre-oxidation of the steam generator [15] to build up an oxide barrier have been considered and tested in the laboratory only. The ability to predict the locations and magnitude of crud buildup, while constantly improving using industry codes like EPRI's BOA [16] and CASL's MAMBA [17], is not high enough to adequately plan for its incidence. Therefore, solutions to completely eliminate the buildup of crud are sought to end these issues.

In this paper, we present experimental results to quantify the crud resistance of different potential fuel cladding coatings. These coatings, chosen for their surface chemical properties as well as their neutronic and chemical compatibility with conditions in a LWR core, were tested using an integrated flowing corrosion loop at PWR conditions to quantify relative amounts of crud surface coverage reduction. The results yield two candidate coatings, TiC and ZrN, which greatly reduce the buildup of crud. Van der Waals (VDW) theory is presented as an explanation for the results, and the data show enough agreement with theoretical predictions to suggest that VDW forces, specifically the induced-dipole force component, is the dominant mechanism of the adhesion of crud to fuel cladding and coatings.

2. Background

Crud, like all fouling deposits, must begin with the adhesion of a first layer to a clean substrate surface. In the case of nuclear reactor fuel, this substrate consists of zirconia (ZrO_2), in a mixture of its tetragonal and monoclinic forms. The crud itself consists mainly of nickel and iron oxides, in particular sub-stoichiometric trevorite ($NiFe_2O_4$), and nickel oxide (NiO) [18]. Reports of Ni metal [19], zirconia [20], and bonaccordite (Ni_2FeBO_5) [21] in PWR crud also exist. Specific material properties, such as the surface energy or the Hamaker constant [22], should dictate to what degree materials will adhere to each other in certain conditions should Debye forces or electrochemical double layers not significantly impact the result. Atomistic studies have provided insight as to whether these Debye forces or a combined DLVO force is required to describe the interactions between crud and fuel cladding. A study by Christensen and Carter [23] showed that the monoclinic ZrO_2 surface is unlikely to be solely cation or anion terminated, due to the long-range electrostatic forces that would render the surface metastable. It is these polar surfaces, charged predominantly with one sign or the other, that would induce the formation of an electrochemical double layer that could contribute noticeably to attraction or repulsion. One of the principal crud phases, NiO, has been shown to undergo octopolar reconstruction from a perfectly cation- or anion-terminated (111) facet, yielding nanofaceted regions 1.5 nm wide with opposite surface terminations [24]. These were deduced by studying the adsorption of NO to the NiO surface. Therefore, the area-averaged charge neutrality of both the monoclinic ZrO_2 and most stable NiO surfaces suggests that a net attraction or repulsion from an electrochemical double layer would not be a dominant force in crud adhesion.

The Hamaker constant A_{afb} describes the induced-dipole based adhesion by van der Waals (VDW) forces, in the case of two materials (a and b) interacting with an intervening fluid (f) [22]:

$$A_{afb} = \left(\sqrt{A_{ava}} - \sqrt{A_{fvf}}\right)\left(\sqrt{A_{bvb}} - \sqrt{A_{fvf}}\right) \quad (1)$$

where A_{ava}, A_{bvb}, and A_{fvf} are the vacuum Hamaker constants for material a, material b, and the fluid f respectively [25]. Calculations of these Hamaker constant is normally quite complex, requiring the application of full Lifshitz integrals [26]

and complete knowledge of the optical (dielectric, refractive) properties of each material [25]. However, simplifications can be made in certain circumstances, especially when the refractive index of all materials involved is relatively low, below 1.7 [27]. Using the Tabor-Winterton approximation (TWA) [28], each of these vacuum Hamaker constants can be written as follows [22], assuming the simplification of a single dominant electron oscillation frequency in the ultraviolet (UV) range [29]:

$$A_{ava}^{TWA} = \frac{3}{4} k_B T \left(\frac{\epsilon_a - 1}{\epsilon_a + 1} \right)^2 + \frac{3\pi\hbar\nu_e}{8\sqrt{2}} \frac{(n_a - 1)^2}{(n_a + 1)^{3/2}} \quad (2)$$

where k_B is Boltzmann's constant, T is the temperature in Kelvin, ϵ is a dielectric constant of a given material, $\hbar$ is Planck's constant, ν_e is the UV plasma oscillation frequency, and n is the index of refraction using the low-frequency limit of a material, taken in the visible-UV range [25]. Here the first term represents the zero-level energetic (electrostatic) contribution to adhesion, and is often ignored as its value rarely approaches over 5% of the Hamaker constant for a system without static charge, while the second term represents attraction or repulsion due to electron oscillations between the materials and the intermediating fluid or vacuum. The dielectric constant and refractive index of a vacuum, both unity, have been substituted here for simplicity. Finally, the Hamaker constant is directly proportional to the VDW force (F_{VDW}) between a spherical particle of crud of diameter d and a substrate, separated by a distance z, in any medium:

$$F_{VDW} = \frac{-A_{Ham} d}{6z^2} \quad (3)$$

Therefore, simply knowing the visible-UV refractive index of a material gives a hint as to whether it should be "sticky" or not. With a refractive index of 2.15 [22], ZrO_2 has a TWA vacuum Hamaker constant of 264.8 zJ, a considerably high value. This value corresponds well to the frequent observation of crud adhering to the zirconia scale always present on Zircaloy-based nuclear fuel rods. By contrast, the carbides and nitrides of Zr and Ti (which is chemically very similar to Zr) show considerably reduced refractive indices [30], and therefore likely lower Hamaker constants leading to less crud adhesion. Table 1 summarizes the known dielectric constants, indices of refraction, and vacuum Hamaker constants for a number of materials under consideration in this study, chosen for their high hardness, low neutron cross sections, and commercial availability. Long-term chemical compatibility with a PWR environment was considered, though not as strongly, so as to more expeditiously test the hypothesis of why crud sticks to fuel cladding. All of these coatings can be applied using conventional techniques, such as plasma ion infiltration or magnetron sputtering.

Material	$\mathbf{n_{633}}$	$\mathbf{n_{210}}$	$\mathbf{A_{ava}}$ (**zJ**)
H_2O, STP	1.332 [31]	1.41 [31]	37 [22]
H_2O, PWR	1.224 [32][1]	—	16.5
ZrO_2	2.24 [33][2]	2.39 [33]	270 [22]
ZrN	0.44 [34]	—	—
ZrC	—	—	—
TiO_2	2.583[35]	1.95 [36]	430 [22]
TiN [3]	1.351 [30]	1.89 [30]	—
TiC [3]	3.079 [30]	1.54 [30]	—
TiB_2	—	—	—
MgO	1.735 [37]	—	120 [38]
Al_2O_3	1.766 [39]	1.79 [39]	150 [22]

Table 1: Known optical properties for the materials in this study. n_{633} - Index of refraction at 633 nm. n_{210} - Index of refraction at 210 nm. A_{ava} - Vacuum Hamaker constant. [1]Quadratically extrapolated from liquid phase data at 320ºC from [32]. [2]Data for monoclinic ZrO_2, average of two birefringent directions. "—" Not found or unavailable. [3]Data for the (111)-terminated face is used, according to [40].

It is unknown, however, whether a simple measurement of adhesion or Hamaker constant in standard laboratory conditions, whether in vacuum or in water, will translate directly to the desired engineering property of enhanced fouling resistance. One study by LeFevre and Jolivet has performed calculations to support this idea specifically in PWR conditions [41], but no study was found that experimentally tests it. They also explicitly note the surprising scarcity of full spectral refractive or dielectric data to perform these calculations. This study seeks to determine the fitness of predicting crud resistance by optical material properties, in an integrated test as similar to the environment found within a PWR as can be reasonably achieved.

3. Experimental Methods

All recordings from loop instrumentation, raw and processed data, spreadsheets for figure generation, and other files used in the creation of the results in this study can be found permanently hosted on our GitHub repository [42].

3.1. Sample Preparation

The nine materials given in Table 1 were chosen for all experiments in this study, based on chemical compatibility with Zircaloys, low neutron cross sections, high hardnesses, and representing a variety of surface energies. It was initially hypothesized that surface energy would be the controlling variable in determining crud resistance, this

Mat'l	$t_{sputter}$ (min.)	Ar	O_2	N_2	RF (V)
		(cm^3/min.)			
ZrO_2	75	38	2	—	—
ZrN	15		—	2	-108
ZrC	7		—	—	—
TiO_2	108		2	—	—
TiN	18.75		—	2	-86
TiC	52.5		—	—	—
TiB_2	12.5		—	—	—
MgO	42		2	—	—
Al_2O_3	75		2	—	—

Table 2: PVD process parameters for each material used in this study

proved not to be the case. In all cases, test substrates were applied to 12.5 mm long, 17.5 mm inner diameter, and 0.2-0.3 mm thick 316 stainless steel rings for integrated flowing loop tests. The rings were mechanically and electrochemically polished to a mirror finish of <50 nm, and sonicated in acetone and ethanol for five minutes each to remove surface contaminants. Physical vapor deposition (PVD) was performed by PVD Products, Inc., to produce coatings roughly 50 nm thick. The exact coating thickness is unimportant provided that it is at least 10 nm thick, to avoid any effect of the underlying substrate changing adhesion. Israelachvili notes that VDW forces are dominated by the coating material in a coating-substrate system, for separation distances on the order of or smaller than the thickness of the coating [22]. Sputtering targets for each material were sourced with at least a 99.99% purity in the form of two-inch diameter discs 1/8th inch thick, bonded to a 1/8th inch disc of pure copper. All substrates were held at a distance of 3.5" from the sputtering target at room temperature, and utilized a 75 W radiofrequency (RF) source at 13.56MHz with a baseline pressure of less than $2.0 \cdot 10^{-6}$ Torr. Pressure was maintained at 5 mTorr for all depositions. Specifics for each material's PVD process parameters are listed in Table 2. Only one hemicylinder of each ring was coated, to ensure a built-in control surface on every specimen. This is due to tiny variations in ring diameter leading to differences in thermal contact, which despite our best efforts to make uniform within the tolerances of our machining tools, still resulted in slight differences in the tactile sliding friction when loading each ring onto the heater rod.

3.2. Flowing PWR Loop Tests

The newly constructed Internally Heated Testloop for PWRs (IHTFP) facility [43] was used for all flowing loop tests. Figure 2 shows a diagram and set of conditions used in the IHTFP, showing that all conditions except for Reynold's number and mass flux can be made identical to those found in PWRs. In these experiments, the system pressure was reduced to 11.5 MPa, resulting in a calculated water saturation temperature of 321C. This was done to avoid heater rod burnout, based on previous tests at 15.5 MPa experiencing such burnouts. Greatly increased nanoparticulate (8-20 nm) NiO crud precursor concentrations of 27.5 parts per million weight (ppmw) and 50.0 ppmw were used in the first and second experiments, respectively, to accelerate crud growth to the days-to-weeks timeframe. A pair of experiments were conducted at these conditions, one for four days, one for thirteen days.

The circulation water for these experiments was mixed in a 100 liter tank connected to the circulation loop. This was first filled with >15 MΩ/cm deionized water by evacuating the loop and using vacuum suction to draw the water in from the water storage tank, and then circulated through a mixed bed ion exchange filter and continuously measured until the water's electrical conductivity was below 0.09 μS/cm. The vacuum filling method was performed to ensure no gas bubbles would remain in the system, which would store energy when pressurized or interfere with measurement equipment. 99.999% dry argon was then bubbled through the tank until the dissolved oxygen concentration was maintained below 200 parts per billion (ppb). Then, 1,400 ppmw of boric acid was added to the tank, and LiOH was added until the pH of the solution reached 7.0. This amounted to 2.2 ppmw of LiOH during these tests. A Mettler-Toledo Thornton 770Max Pure Water Smart Sensor was used to measure pH, dissolved oxygen, and water conductivity. Water chemistry conditions were controlled and monitored according to the Electric Power Research Institute's (EPRI's) PWR water chemistry guidelines [44].

The IHTFP loop was heated using a combined 4,992 W of strip heaters and one vertical, internally heated, electrically isolated 1,750 W heater rod, yielding a nominal heat flux of 206 kW/m^2 during these tests. This is lower than the PWR core average, and is only suitable for relative comparisons of crud resistance, not absolute crud growth rates. Up to twelve different rings, each containing one half-coated ring of each material, were used to enable direct comparison of crud coverage for materials in identical test conditions. These half-coated samples were specifically used to correct for any slight differences in heat flux, thermal contact, flow velocity, or other localized environmental conditions. By comparing relative amounts of crud coverage between the coated and uncoated halves of each sample, the effectiveness of each coating at reducing crud surface coverage can be more uniformly compared. Figure 3 shows

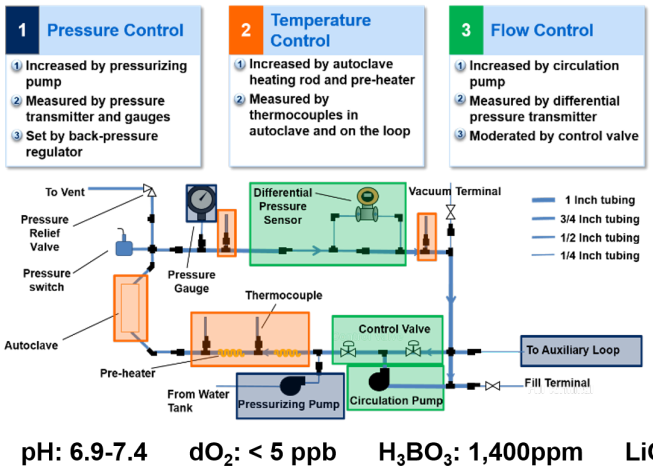

	PWR	IHTFP
Pressure	15.5 MPa	15.5 MPa
Temperature	287-324°C	320°C
Reynolds No.	$5 \cdot 10^5$	$1.62 \cdot 10^5$
Mass flux	3500 kg/m^{2}s	1920 kg/m^{2}s
Fe_3O_4, NiO	0.01 - 0.1 ppm	10 - 100 ppm

pH: 6.9-7.4 dO_2: < 5 ppb H_3BO_3: 1,400ppm LiOH: 2.2ppm H_2O Conductivity: <0.3 µS/cm

Figure 2: Diagram and experimental conditions in the IHTFP flowing tests

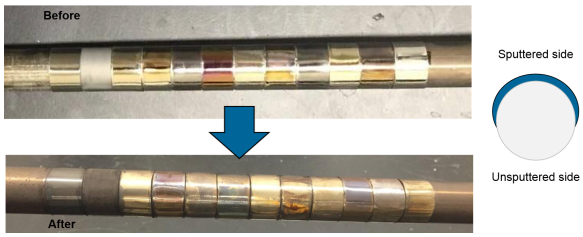

Figure 3: (Left) Images of specimen rings before and after the one-week tests, showing differences in crud coverage. (Right) Schematic showing how each specimen ring was half-coated, to ensure a built-in control surface for every specimen in every test.

images of the specimen rings on a heater rod, after press-fitting to ensure good thermal contact. Following flowing exposure in the IHTFP loop, specimens were extracted from the heater rod using a Dremel tool, and sectioned into control and coated halves near the control/coated delineation for scanning electron microscope (SEM) analysis.

The presence of sub-cooled boiling was confirmed using both calculations and direct experimental evidence. Kandlikar developed criteria for the onset of sub-cooled boiling [45], relating the system pressure, liquid sub-cooling, and flow parameters to the necessary wall superheat temperature. It can be seen that for reasonable surface roughness, only a 1°C wall superheat is required to induce sub-cooled boiling. In reality the IHTFP tests were conducted at 2-3°C to avoid circulation pump cavitation, still requiring a 1-2°C wall superheat. The superheat temperature of the samples in these experiments was calculated to be 2.7°C using the Thom correlation [46]:

$$\Delta T_{sat} = 22.5\sqrt{q''}e^{\left(\frac{-P}{8.7}\right)} \quad (4)$$

where ΔT_{sat} is the wall superheat in Kelvin, q" is the heat flux in $^{MW}/_{m^2}$, and P is the system pressure in MPa. Therefore enough wall superheating exists to induce sub-cooled boiling. Direct experimental evidence of some of the thickest crud grown in these experiments (shown in Figure 4) also exhibits numerous boiling chimneys, which are direct evidence of sub-cooled boiling.

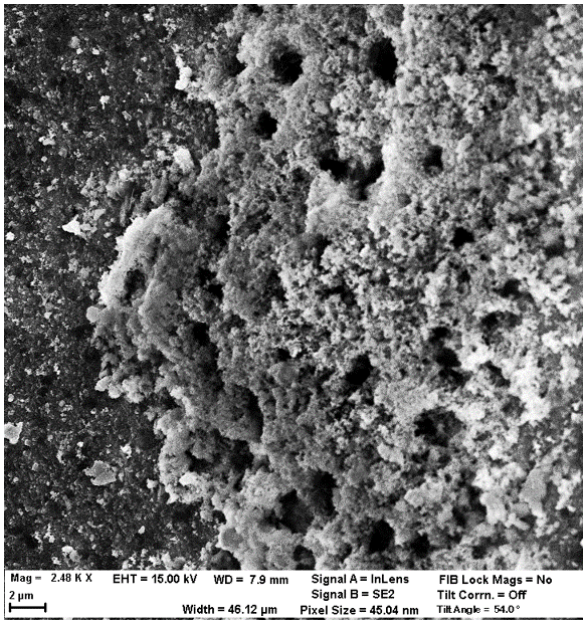

Figure 4: SEM image of crud grown in the IHTFP facility, exhibiting numerous boiling chimneys indicative of sub-cooled boiling

3.3. SEM Image Analysis

The goal of the image analysis was to quantify the relative percentage reduction in crud coverage between the coated and control surfaces of each specimen. To automate this process, image processing algorithms were used to binarize each SEM image into crud and non-crud surfaces, allow-

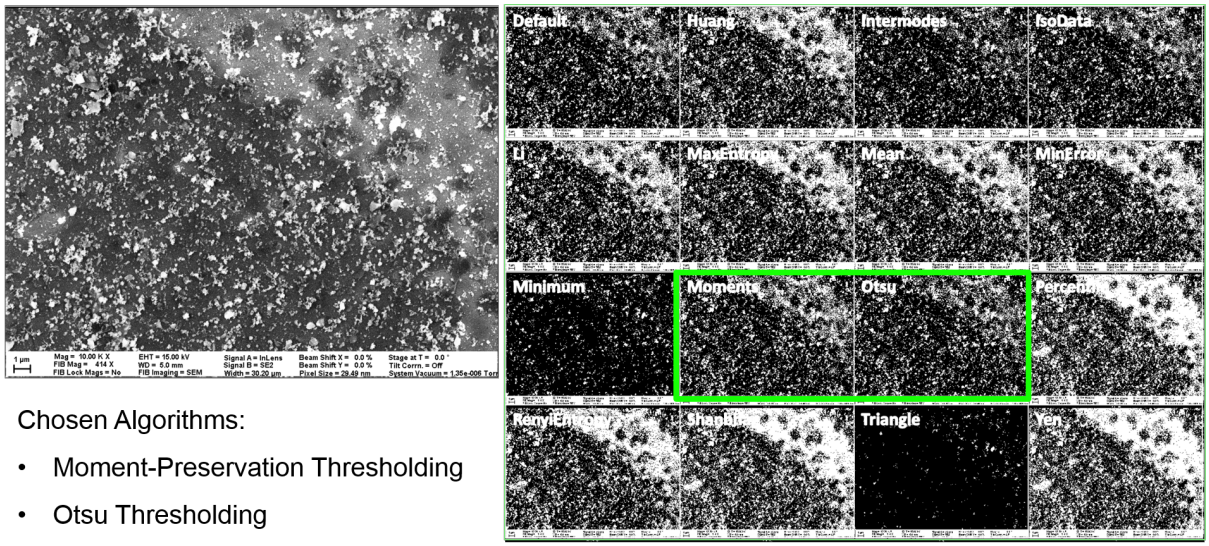

Figure 5: Example training image with binarized results from sixteen image processing algorithms

ing easy determination of how much crud existed on a surface. Sixteen image processing algorithms present in the ImageJ software package were tested using a series of five trial images from the complete dataset. The experimenters determined which of the algorithms reliably binarized only the crud, and not other artifacts in the images, by training the sixteen image processing algorithms of a set of ten testing images. Zooming in to the light regions of each image revealed which areas contained crud-like small particulates, while EDX analysis in a JEOL 5910 SEM confirmed the presence of high levels of Ni, occasionally with Fe present. Regions without these two metals were deemed not to be crud, as none of the coatings contained them. Figure 5 shows this process in detail, revealing that the Moment Preserving [47] and Otsu [48] thresholding algorithms best isolated crud with minimal false positive identification of features. Ten SEM images at 10,000x magnification in secondary electron (SE) mode were taken using a Zeiss NVision 40 dual-beam SEM/FIB on each control and each coated surface of every specimen from both experiments, at distances at least one millimeter apart to ensure representative surface coverage. Both image processing algorithms were used to determine the percentage crud coverage on each material's coated and control surfaces. This was done to ensure that the choice of the image processing algorithm did not noticeably affect the results.

4. Results

Table 3 summarizes the crud coverage percentages for every control and coated surface in this study, while Figure 6 presents the results graphically. As can be seen in the figure, three materials reliably reduced the crud coverage fraction beyond experimental error. In the cases of TiC and ZrN, this reduction in coverage was 40%, a significant reduction in crud adhesion. Error bars in Figure 6 were generated by summing the averaged errors for each material's coated and control surfaces in quadrature, averaging across the two experiments, and doubling that value to obtain quadrature-averaged 95% confidence intervals. As should be expected, ZrO_2 showed no statistically significant change in crud coverage. Notable results include repeatable crud reduction with 95% confidence by ZrN, TiN, TiC, and repeatable increases in crud coverage by TiO_2, and MgO across both experiments and both image processing techniques. Two materials, ZrO_2 and Al_2O_3, showed an increase in crud coverage between coated and control surfaces in one experiment and a decrease in another. This may be attributable to different absolute heat fluxes between experiments, as each sample ring will have a sightly different dimension and therefore thermal fit. The doubled crud precursor concentration between experiments is not expected to noticeably affect results, and no significant deviation between experiments was observed. The choice of image processing never changed the sign of crud coverage except in the case of Al_2O_3, but not within the limits of experimental error. However, as can be seen in Table 3 and Figure 6 it did somewhat change the magnitude of observed crud coverage in some cases. This is why both were used, to ensure that the choice of image processing algorithm did not noticeably affect the final results. Finally, it should be noted that while the precursor concentration in the second experiment was almost doubled, absolute surface coverages were uniformly lower. This can be attributed to either the continued passivization of the loop itself during operation, reducing

	Experiment 1 (27.5 ppm NiO)				Experiment 2 (50.0 ppm NiO)			
Algorithm	**Moment Preserving**		**Otsu**		**Moment Preserving**		**Otsu**	
Material	Control	Coated	Control	Coated	Control	Coated	Control	Coated
ZrO_2	61.3 ± 7.9	51.4 ± 4.4	58.6 ± 7.9	46.8 ± 4.3	25.9 ± 2.5	36.2 ± 1.4	21.8 ± 4.3	27.3 ± 1.7
ZrN	47.0 ± 15.9	34.1 ± 3.9	45.8 ± 19.1	24.2 ± 4.8	31.2 ± 1.3	20.7 ± 0.2	22.2 ± 2.4	13.5 ± 0.6
ZrC	41.5 ± 11.8	33.2 ± 6.4	33.3 ± 10.1	32.4 ± 5.7	25.8 ± 0.4	23.9 ± 0.6	16.8 ± 1.0	15.7 ± 1.0
TiO_2	53.4 ± 3.6	54.0 ± 3.6	30.8 ± 4.5	52.9 ± 2.9	25.9 ± 0.4	33.7 ± 0.5	17.0 ± 1.3	22.1 ± 0.5
TiN	58.0 ± 9.3	49.1 ± 1.7	55.0 ± 10.4	47.6 ± 2.9	19.7 ± 0.2	16.6 ± 0.2	14.8 ± 0.9	12.4 ± 0.2
TiC	63.6 ± 11.0	44.6 ± 1.4	60.6 ± 13.3	43.2 ± 2.9	35.3 ± 6.3	18.4 ± 0.5	29.6 ± 8.2	13.8 ± 2.3
TiB_2	54.0 ± 2.9	62.9 ± 2.1	50.0 ± 1.9	58.7 ± 2.1	42.7 ± 8.1	44.9 ± 0.7	34.4 ± 8.3	37.2 ± 1.4
MgO	42.4 ± 2.4	49.7 ± 1.5	38.0 ± 6.4	47.0 ± 2.0	24.7 ± 0.5	33.5 ± 2.2	19.4 ± 0.9	24.8 ± 1.7
Al_2O_3	38.4 ± 5.7	45.1 ± 7.1	32.7 ± 5.4	43.0 ± 9.7	36.9 ± 8.3	26.2 ± 0.5	30.8 ± 8.6	21.8 ± 0.6

Table 3: Percentage crud coverages for all control and coated surfaces in this study, as measured by SEM and image analysis

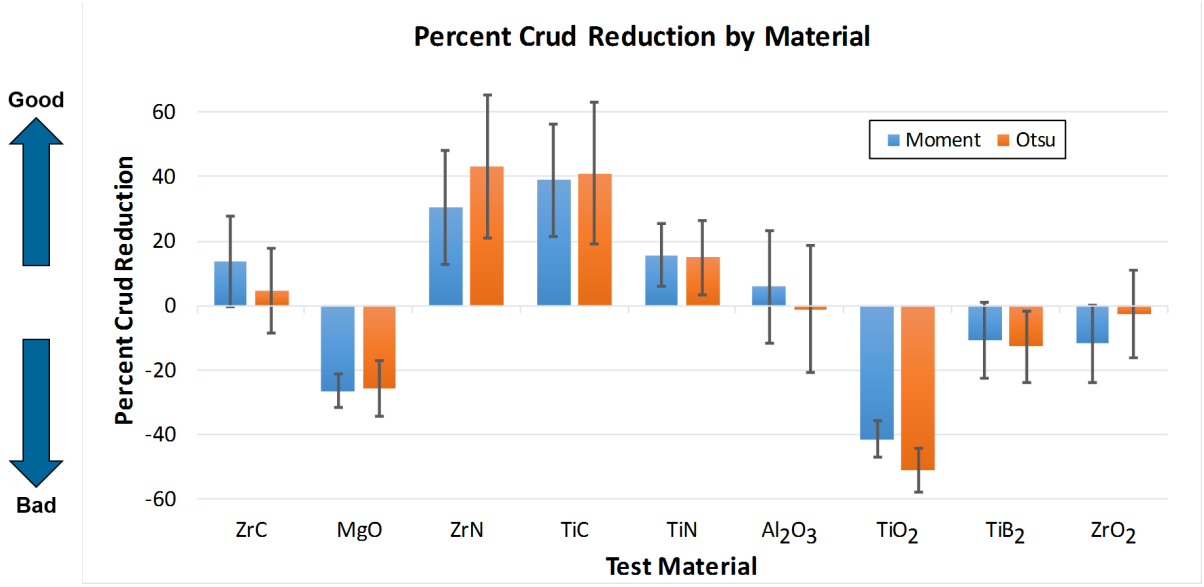

Figure 6: Relative reductions in crud coverage for the nine materials in this study, along with quadrature-averaged 95% confidence intervals in the measurements

the natural crud source term, or to differences in thermal fit and therefore sub-cooled boiling heat fluxes between experiments. It was noticed that each sample ring required a different sliding force to reach its position on the heater rod (all samples required considerable force to attach). Therefore, slight differences in the machined tolerances of each sample ring and each heating rod could have led to this difference in *absolute* crud coverage, by way of small differences in heat fluxes and wall superheat temperatures.

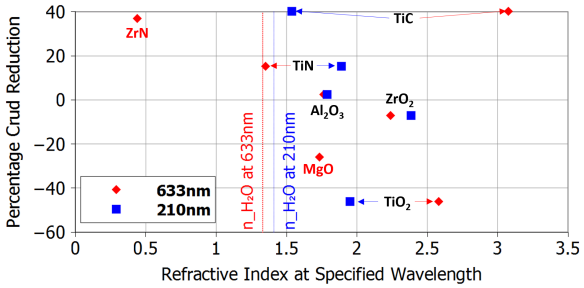

Figure 7: Comparison of percentage crud reduction in loop testing experiments vs. refractive index at two chosen wavelengths

5. Discussion

The data demonstrate that two materials, ZrN and TiC, were repeatably able to resist surface formation of crud in a PWR-representative environment by 40% with high confidence. One other material, TiN, performed satisfactorally within margins of error. The major conclusions are insensitive to the type of image processing algorithm used, and to the fluctuations in loop chemistry which are more extreme than those found in commercial PWRs. None of the other six materials tested resisted crud formation appreciably, while two (MgO and TiO_2) appeared to encourage it. TiO_2 has specifically been used to protect jet pump nozzle assemblies and inlet flow mixers in boiling water reactors (BWRs) [49], so its poor performance in this study raises the question of why it did not help. Dulka et al specifically used hard, electrically insulating ceramics such as TiO_2 and Ta_2O_5 to eliminate any electrostatic deposition of charged particulates floating in the BWR water, and it appears to have worked.

These data bring forth an obvious question: Do Van der Waals forces, specifically London dispersion forces, contribute most significantly to crud formation in PWRs? If the answer is yes, then it provides a convenient theoretical basis for the design of crud-resistant materials, provided the chosen materials are also hard, neutronically transparent, stable in PWR water, and resistant to radiation damage. The success of the work of Dulka et al does not preclude the existence of charged particulates in PWR water, which would interact with cladding materials via dipole-induced-dipole (Debye) forces, which are much stronger than induced-dipole-induced-dipole (London dispersion) forces. However, their study did demonstrate that these Debye forces can be masked using an electrical insulator, which is not highly electrostatically polarizable. In addition, the poor performance of TiO_2 in this study suggests a link between London dispersion forces and crud deposition, as masking the cladding in a manner nearly identical to that of Dulka et al did not prevent fouling.

A direct comparison of the percentage crud reduction with the visible refractive index, used in determining the TWA Hamaker constant, is given in Figure 7. A generally negative trend can be seen for the refractive index at both 633 nm (red) and 210 nm (ultraviolet) vs. the percentage crud reduction measured in this study, with one notable exception. Titanium carbide (TiC), despite having the highest refractive index at 633 nm, also demonstrated the most resistance to crud formation. All materials with tabulated data at a more ultraviolet wavelength of 210 nm (Al_2O_3, TiC, TiN, TiO_2, monoclinic ZrO_2) exhibited a marked negative correlation between refractive index at 210 nm and percentage crud reduction. This initially simple comparison points to more complexity required to fully explain the results.

The basis of the Tabor-Winterton approximation (TWA) is that for materials with low refractive indices ($n<1.7$), one can simply use a single value of the refractive index, commonly chosen at 633 nm (the emission line of a He-Ne laser), to approximate the full spectral Hamaker constant [27]. This has been verified by calculating both the TWA and full spectral Hamaker constants for a number of materials, and comparing with experimental measurements [22]. However, it appears that the TWA is really only valid for material-fluid-material systems whose indices of refraction vary in similar ways across the relevant parts of the spectrum, known to be the visible and ultraviolet ranges. A more detailed comparison of the refractive indices of seven of the tested materials whose refractive index spectra are known in this range is shown in Figure 8. Now the comparison becomes more clear, as the seven materials with known refractive index spectra roughly line up in order of increasing crud resistance vs. the difference in their UV refractive index spectra compared with water. In particular, TiC and ZrN show either near parity or a negative value in this relative refractive index spectrum in much of the near-UV region, agreeing with previous studies suggesting that this near-UV region is quite

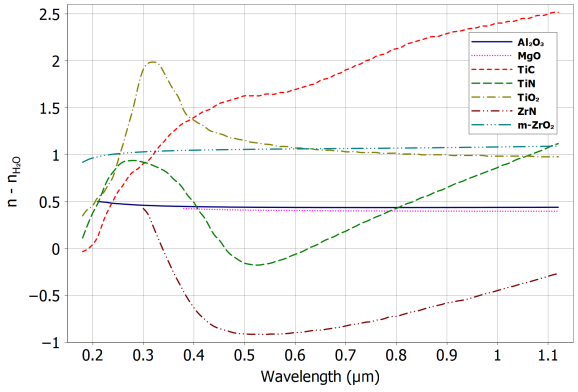

Figure 8: Comparison of percentage crud reduction in loop testing experiments vs. refractive index spectra in the visible and near UV/IR ranges. The difference in the refractive index vs. that of water for each material is plotted for a more meaningful comparison. Full spectral refractive index data sourced from [39] (Al_2O_3), [31] (H_2O), [37] (MgO), [30] (TiC & TiN), [36] (TiO_2), and [33] ($m - ZrO_2$), where 'm' stands for monoclinic.

important in determining the Hamaker constant [50, 25]. The negative relative refractive index of ZrN in particular suggests VDW repulsion at these wavelengths, which has been shown in previous systems [50]. This, combined with the previously stated evidence of static charges not being dominant when metallic surfaces are coated with electrical insulators [49], suggest that the induced-dipole component of VDW forces is the controlling variable in designing crud-resistant materials.

The major shortcoming in the current ability to design crud-resistant materials from theory is the availability of refractive index spectra in the near to far-UV range. Many of the data, despite being quite current, are simply not measured beyond the 100nm range due to the low wavelength cutoff of the deuterium arc lamp emission spectrum of 112 nm, the most common UV excitation source used in UV-vis-IR spectrometers. Either a lower wavelength UV source is required to determine these fuller refractive index spectra, or electronic excitation techniques such as valence electron energy loss spectroscopy (VEELS) can be used [51]. These measurements are quite feasible, it becomes a matter of turning our attention to experimental measurements of these and similar materials for the purpose of designing better crud-resistant material coatings.

6. Conclusions and Future Work

It was hypothesized that matching the optical properties of fuel cladding coatings to the surrounding water would impart resistance to crud formation. This hypothesis appears to have been supported by integral loop tests, and a qualitative comparisons of known, experimental refractive index spectra with that of water. In particular, TiC and ZrN were both found to reduce roughly 40% of crud deposition in two experiments with 95% confidence compared to uncoated control surfaces. Direct measurement of adhesion values in PWR-chemistry water and of the vacuum Hamaker constants of potential materials will confirm these integral tests and theoretical predictions, respectively. It is recommended to dedicate more resources to the experimental measurement of adhesion forces for these and similar coatings in the atomic force microscope (AFM), and to measure the refractive index spectra in the near-UV range (10-400 nm), to verify whether true full spectral refractive index comparison is a satisfactorally quantitative metric for designing crud-resistant materials. Future work should also consider determining the optimum thickness of the coatings/surface pretreatments to ensure the coating remains stable while the fuel rod heat flux sustains sub-cooled nucleate boiling.

The next steps for demonstrating the true effectiveness of these potentially crud-resistant coatings is in-reactor testing, where the material coatings, applied to prototypical ZIRLO or other Zircaloy coupons, will be exposed to flowing water at PWR conditions with radiolysis. This is a necessary step in testing crud resistance in a true reactor environment, as the coatings must both survive the test and continue functioning before testing as a lead test rod (LTR) could take place in a commercial reactor. These experiments are planned for the coming year, with an LTR campaign to follow in 2019 pending success. A parallel effort includes direct measurement of adhesion forces in the AFM, and the construction of a high-temperature, hyperbaric AFM for direct measurements of Hamaker constants in water at PWR conditions. Finally, continued analysis of the structure and chemistry of the crud formed in these experiments can help validate thermodynamic predictions, models of crud's effects, and experimental observations. These include the prediction that boron incorporates into the Ni-bearing phases of crud [52], verifiable by x-ray diffraction (XRD) analysis, cross-sectional fractal analysis of the structure of crud to validate assumptions made in models of crud's effects on cladding [53], and searching for phases like bonaccordite ($Ni2FeBO_5$) observed in PWRs [54].

Acknowledgments

Particular thanks are due to the Electric Power Research Institute (EPRI), for funding this work from its inception through loop testing under their Polaris and PWR Technical Advisory Committee (P-TAC) programs on contract numbers 10002739,

10004433, and 10005086. Thanks are also due to the MIT Center for Advanced Nuclear Energy Systems (CANES), an MIT Energy Initiative (MITEI) Low-Carbon Energy Center (LCEC), for providing support for the loop testing autoclave, and to the MIT-Japan Hayashi Seed Grant for providing seed funds for this work. The authors also acknowledge James Greer and Adam Shepard from PVD Products, Inc. for sputtering services and disclosure of the PVD process parameters, and W. Art Byers, Zeses Karoutas, Guoqiang Wang, and Peng Xu of the Westinghouse Electric Company for many useful discussions.

[1] P. L. Frattini, J. Blok, S. Chauffriat, J. Sawicki, and J. Riddle. Axial offset anomaly: coupling PWR primary chemistry with core design. *Nucl. Ener.*, 40(2):123–135, 2001.

[2] A. Kunkle and D. Testa. The westinghouse pressurized water reactor nuclear power plant. Technical report, Westinghouse Electric Division, 1984. Accessed at http://www4.ncsu.edu/∼doster/NE405/Manuals/PWR_Manual.pdf on 2017-04-30.

[3] F. Carrette, M. C. Lafont, G. Chatainier, L. Guinard, and B. Pieraggi. Analysis and TEM examination of corrosion scales grown on alloy 690 exposed to pressurized water at 325°C. *Surf. Interface Anal.*, 34(1):135–138, 2002.

[4] R. Molins, M. Pijolat, M. Sennour, L. Marchetti, S. Perrin, and O. Raquet. Characterization of the oxide films formed at the surface of ni-base alloys in pressurized water reactors primary coolant by transmission electron microscopy. *Mater. Sci. Forum*, 595:539–547, 2008.

[5] M. P. Short, D. Gaston, C. R. Stanek, and S. Yip. A perspective on coupled multiscale simulation and validation in nuclear materials. *MRS Bulletin*, 39(1):71–77, 2014.

[6] J. Deshon, D. Hussey, B. Kendrick, J. McGurk, J. Secker, and M. P. Short. Pressurized water reactor fuel crud and corrosion modeling. *JOM*, 63(8):64, 2011.

[7] J. Henshaw, J. C. McGurk, H. E. Sims, A. Tuson, S. Dickinson, and J. Deshon. A model of chemistry and thermal hydraulics in PWR fuel crud deposits. *J. Nucl. Mater.*, 353(1-2):1–11, 2006.

[8] Y. H. Jeong, J. H. Baek, S. J. Kim, H. G. Kim, and H. Ruhmann. Corrosion characteristics and oxide microstructures of Zircaloy-4 in aqueous alkali hydroxide solutions. *J. Nucl. Mater.*, 270(3):322–333, 1999.

[9] J. Deshon et al. Fuel reliability guidelines: PWR fuel cladding crud and corrosion. Technical Report 1015499, Electric Power Research Institute (EPRI), Palo Alto, CA, USA, 2008.

[10] M. P. Short, D. Hussey, B. K. Kendrick, T. M. Besmann, C. R. Stanek, and S. Yip. Multiphysics modeling of porous CRUD deposits in nuclear reactors. *J. Nucl. Mater.*, 443(1-3):579–587, 2013.

[11] I. ul Haq, N. Cinosi, M. Bluck, G. Hewitt, and S. Walker. Modelling heat transfer and dissolved species concentrations within PWR crud. *Nucl. Eng. Des.*, 241(1):155–162, 2011.

[12] J. Blok, P. Frattini, D. Gross, and T. Moser. Advances in ultrasonic fuel cleaning. In *Proceeding of Societe Francaise d'Energie Nucleaire - SFEN, Fontevraud 5 International symposium*, 1-2, pages 547–553, Fontevraud - Royal Abbey (France), 2002.

[13] R. Yang, B. Cheng, J. Deshon, K. Edsinger, and O. Ozer. Fuel R & D to improve fuel reliability. *J. Nucl. Sci. Technol.*, 43(9):951–959, 2006.

[14] W. A. Byers, D. V. Paramonov, M. B. Dzodzo, Z. E. Karoutas, and M. Y. Young. Crud-resistant nuclear fuel cladding, 2004. U.S. Patent No, 6813329 B1.

[15] I. Bobin-Vastra, B. Sala, N. Engler, P. Saurin, and M. C. Thiry. Preoxidation of SG alloy 690 tubes to decrease metal release in the primary circuit: A laboratory study. In *8th International Symposium on Environmental Degradation of Materials in Nuclear Power Systems - Water Reactors*, volume 1-2, pages 507–513, Amelia Island, FL, USA, 1997. American Nuclear Society.

[16] EPRI. Boron-induced offset anomaly (BOA) risk assessment tool, version 1.0. Technical Report 1003211, Electric Power Research Institute (EPRI), Palo Alto, CA, USA, 2003.

[17] V. Petrov, B. K. Kendrick, D. Walter, A. Manera, and J. Secker. Prediction of CRUD deposition on PWR fuel using a state-of-the-art CFD-based multiphysics computational tool. *Nucl. Eng. Des.*, 299:95–104, 2016.

[18] J.-W. Yeon, I.-K. Choi, K.-K. Park, H.-M. Kwon, and K. Song. Chemical analysis of fuel crud obtained from korean nuclear power plants. *J. Nucl. Mater.*, 404(2):160–164, 2010.

[19] J. X. Chen. On the interaction between fuel crud and water chemistry in nuclear power plants. Technical Report SKI Report 00:5, Studsvik Material AB, SE-611 82 Nykoping, Sweden, 2000. SKI Report 00:5.

[20] J. A. Sawicki. Evidence of Ni2FeBO5 and m-ZrO2 precipitates in fuel rod deposits in AOA-affected high boiling duty PWR core. *J. Nucl. Mater.*, 374(1-2):248–269, 2008.

[21] J. A. Sawicki. Analyses of crud deposits on fuel rods in PWRs using Mossbauer spectroscopy. *J. Nucl. Mater.*, 402(2-3):124–129, 2010.

[22] J. N. Israelachvili. *Intermolecular and Surface Forces.* Academic Press, San Diego, third edition, 2011. pp. 261, 263, 275, 282-283.

[23] A. Christensen and E. A. Carter. First-principles study of the surfaces of zirconia. *Phys. Rev. B*, 58(12):8050, 1998.

[24] M. Schönnenbeck, D. Cappus, J. Klinkmann, H.-J. Freund, L. G. M. Petterson, and P. S. Bagus. Adsorption of CO and NO on NiO and CoO: a comparison. *Surf. Sci.*, 347(3):337–345, 1996.

[25] L. Bergström. Hamaker constants of inorganic materials. *Adv. Colloid Interface Sci.*, 70:125–169, 1997.

[26] E. M. Lifshitz. The theory of molecular attractive forces between solids. *Sov. Phys.*, 2(1):73–83, 1956.

[27] R. H. French, R. M. Cannon, L. K. DeNoyer, and Y.-M. Chiang. Full spectral calculation of non-retarded hamaker constants for ceramic systems from interband transition strengths. *Solid State Ionics*, 75:13–33, 1995.

[28] D. Tabor and R. H. S. Winterton. The direct measurement of normal and retarded van der waals forces. *Proc. R. Soc. London A: Mathematical, Physical and Engineering Sciences*, 312(1511):435–450, 1969.

[29] V. A. Parsegian. *Van der Waals Forces: A Handbook for Biologists, Chemists, Engineers, and Physicists.* Cambridge University Press, 2005. p. 63. ISBN 978-0511614606.

[30] J. Pflüger, J. Fink, W. Weber, K. P. Bohnen, and G. Crecelius. Dielectric properties of tic_x, tin_x, vc_x, and vn_x from 1.5 to 40 ev determined by electron-energy-loss spectroscopy. *Phys. Rev. B*, 30:1155–1163, 1984.

[31] M. Daimon and A. Masumura. Measurement of the refractive index of distilled water from the near-infrared region to the ultraviolet region. *Appl. Opt.*, 46(18):3811–3820, 2007.

[32] A. H. Harvey, J. S. Gallagher, and J. M. H. Levelt Sengers. Revised formulation for the refractive index of water and steam as a function of wavelength,

temperature and density. *J. Phys. Chem. Ref. Data*, 27(4):761–774, 1998.

[33] N. M. Balzaretti and J. A. H. da Jornada. Pressure dependence of the refractive index of monoclinic and yttria-stabilized cubic zirconia. *Phys. Rev. B*, 52:9266–9269, 1995.

[34] M. Veszelei, K. Andersson, C.-G. Ribbing, K. Järrendahl, and H. Arwin. Optical constants and drude analysis of sputtered zirconium nitride films. *Appl. Opt.*, 33(10):1993–2001, 1994.

[35] J. R. DeVore. Refractive indices of rutile and sphalerite. *J. Opt. Soc. Am.*, 41(6):416–419, 1951.

[36] T. Siefke, S. Kroker, K. Pfeiffer, O. Puffky, K. Dietrich, D. Franta, I. Ohlídal, A. Szeghalmi, E.-B. Kley, and A. Tünnermann. Materials pushing the application limits of wire grid polarizers further into the deep ultraviolet spectral range. *Adv. Opt. Mater.*, 4:1780–1786, 2016.

[37] R. E. Stephens and Irving H. M. Index of refraction of magnesium oxide. *J. Res. Nat. Bureau Standards*, 49(4):249–252, 1952.

[38] L. Bergström, A. Meurk, H. Arwin, and D. J. Rowcliffe. Estimation of hamaker constants of ceramic materials from optical data using lifshitz theory. *J. Am. Ceram. Soc.*, 79(2):339–348, 1996.

[39] I. H. Malitson and M. J. Dodge. Refractive index and birefringence of synthetic sapphire. *J. Opt. Soc. Am.*, 62:1405, 1972.

[40] J. Rohrer and P. Hyldgaard. Ab initio thermodynamics of deposition growth: Surface terminations of TiC(111) and TiN(111) grown by chemical vapor deposition. *Phys. Rev. B*, 82:045415, 2010.

[41] G. Lefèvre and A. Jolivet. Calculation of hamaker constants applied to the deposition of metallic oxide particles at high temperature. In H. Müller-Steinhagen, M. R. Malayeri, and A. P. Watkinson, editors, *Proceedings of International Conference on Heat Exchanger Fouling and Cleaning VIII*, pages 120–124, Schladming, Austria, June 2009.

[42] [Dataset] I. Dumnernchanvanit, N. Q. Zhang, S. Robertson, A. Delmore, M. B. Carlson, D. Hussey, and M. P. Short. Data and code/script repository for 2017 IHTFP loop testing of crud-resistant materials paper, April 2017. GitHub repository. Accessible at https://github.com/shortlab/2017-IHTFP-Loop-Testing Permanent Link at DOI: 10.5281/zenodo.570008.

[43] I. Dumnernchanvanit, N. Zhang, A. R. Delmore, and M. P. Short. Design and assembly of experimental facility for CRUD characterization and mitigation at PWR cladding conditions. *Trans. Amer. Nucl. Soc.*, 111:1579–1582, 2014.

[44] J. Deshon et al. Pressurized water reactor primary water chemistry guidelines: Revision 7, volumes 1 and 2. Technical Report 3002000505, Electric Power Research Institute (EPRI), Palo Alto, CA, USA, 2014.

[45] S. G. Kandlikar. Heat transfer characteristics in partial boiling, fully developed boiling, and significant void flow regions of subcooled flow boiling. *J. Heat Transf.*, 120(2):395–401, 1998.

[46] N. E. Todreas and M. S. Kazimi. *Nuclear Systems Volume I: Thermal Hydraulic Fundamentals, Second Edition*. CRC Press, 2011.

[47] W.-H. Tsai. Moment-preserving thresholding: a new approach. *Computer Vision Graphics and Image Processing*, 19:377–393, 1984.

[48] N. Otsu. A threshold selection method from gray-level histograms. *IEEE Trans. Sys., Man., Cyber.*, 9(1):62–66, 1979.

[49] C. P. Dulka, J. F. Ackerman, D. W. Sandusky, M. O. Lenz, L. L. Lantz, M. B. McMahan, and G. A. MacMillan. Apparatus and methods for protecting a jet pump nozzle assembly and inlet-mixer, 2003. US Patent 6,633,623.

[50] J. Visser. On hamaker constants: A comparison between hamaker constants and lifshitz-van der waals constants. *Adv. Colloid Interface Sci.*, 3(4):331–363, 1972.

[51] R. H. French, C. Scheu, G. Duscher, H. Müllejans, M. J. Hoffmann, and R. M. Cannon. Interfacial electronic structure and full spectral hamaker constants of Si3N4 intergranular films from VUV and sr-veel spectroscopy. *MRS Proc.*, 357:243, 1994.

[52] Z. Rak, C. J. O'Brien, D. W. Brenner, D. A. Andersson, and C. R. Stanek. Understanding the atomic-level chemistry and structure of oxide deposits on fuel rods in light water nuclear reactors using first principles methods. *JOM*, 68(11):2912–2921, 2016.

[53] M. M. Jin and M. P. Short. Multiphysics modeling of two-phase film boiling within porous corrosion deposits. *J. Comput. Phys.*, 316:504–518, 2016.

[54] J. A. Sawicki. Hydrothermal synthesis of Ni2FeBO5 in near-supercritical PWR coolant and possible effects of neutron-induced 10B fission in fuel crud. *J. Nucl. Mater.*, 415(2):179–188, 2011.